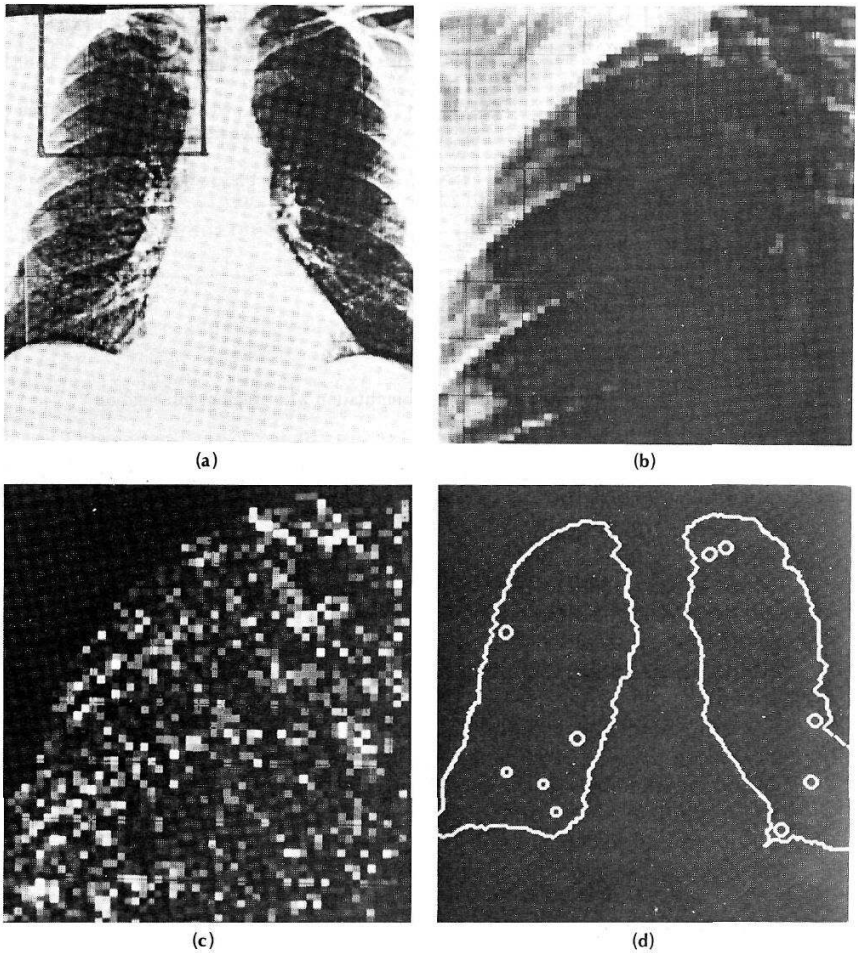

Fig. 4.7 Using the Hough technique for circular shapes. (a) Radiograph. (b) Window. (c) Accumulator array for $r = 3$. (d) Results of maxima detection.

circular boundaries detected by the Hough technique are overlaid on the original image.

4.3.3 Trading Off Work in Parameter Space for Work in Image Space

Consider the example of detecting ellipses that are known to be oriented so that a principal axis is parallel to the x axis. These can be specified by four parameters. Using the equation for the ellipse together with its derivative, and substituting for the known gradient as before, one can solve for two parameters. In the equation

$$\frac{(x-x_0)^2}{a^2} + \frac{(y-y_0)^2}{b^2} = 1 \tag{4.3}$$

x is an edge point and x_0, y_0, a, and b are parameters. The equation for its derivative is

$$\frac{(x-x_0)}{a} + \frac{(y-y_0)^2}{b^2}\frac{dy}{dx} = 0 \tag{4.4}$$

where $dy/dx = \tan\phi(x)$. The Hough algorithm becomes:

Algorithm 4.2: Hough technique applied to ellipses

For each discrete value of x and y, increment the point in parameter space given by a, b, x_0, y_0, where

$$x = x_0 \pm \frac{a}{(1 + b^2/a^2\tan^2\phi)^{1/2}} \tag{4.5}$$

$$y = y_0 \pm \frac{b}{(1 + a^2\tan^2\phi/b^2)^{1/2}} \tag{4.6}$$

that is,

$$A(a, b, x_0, y_0) := A(a, b, x_0, y_0) + 1$$

For a and b each having m values the computational cost is proportional to m^2.

Now suppose that we consider all pairwise combinations of edge elements. This introduces two additional equations like (4.3) and (4.4), and now the four-parameter point can be determined exactly. That is, the following equations can be solved for a unique x_0, y_0, a, b.

$$\frac{(x_1 - x_0)^2}{a^2} + \frac{(y_1 - y_0)^2}{b^2} = 1 \tag{4.7a}$$

$$\frac{(x_2 - x_0)^2}{a^2} + \frac{(y_2 - y_0)^2}{b^2} = 1 \tag{4.7b}$$

$$\frac{x_1 - x_0}{a^2} + \frac{y_1 - y_0}{b^2}\frac{dy}{dx} = 0 \tag{4.7c}$$

$$\frac{x_2 - x_0}{a^2} + \frac{y_2 - y_0}{b^2}\frac{dy}{dx} = 0 \tag{4.7d}$$

$$\frac{dy}{dx} = \tan\phi \qquad \left(\frac{dy}{dx} \text{ is known from the edge operator}\right)$$

Their solution is left as an exercise. The amount of effort in the former case was proportional to the product of the number of discrete values of a and b, whereas this case involves effort proportional to the square of the number of edge elements.

4.3.4 Generalizing the Hough Transform

Consider the case where the object being sought has no simple analytic form, but has a particular silhouette. Since the Hough technique is so closely related to template matching, and template matching can handle this case, it is not surprising that the Hough technique can be generalized to handle this case also. Suppose for the moment that the object appears in the image with known shape, orientation, and scale. (If orientation and scale are unknown, they can be handled in the same way that additional parameters were handled earlier.) Now pick a reference point in the silhouette and draw a line to the boundary. At the boundary point compute the gradient direction and store the reference point as a function of this direction. Thus it is possible to precompute the location of the reference point from boundary points given the gradient angle. The set of all such locations, indexed by gradient angle, comprises a table termed the R-table [Ballard 1981]. Remember that the basic strategy of the Hough technique is to compute the possible loci of reference points in parameter space from edge point data in image space and increment the parameter points in an accumulator array. Figure 4.8 shows the relevant geometry and Table 4.1 shows the form of the R-table. For the moment, the reference point coordinates (x_c, y_c) are the only parameters (assuming that rotation and scaling have been fixed). Thus an edge point (x, y) with gradient orientation ϕ constrains the possible reference points to be at $\{x + r_1(\phi) \cos [\alpha_1(\phi)],\ y + r_1(\phi) \sin [\alpha_1(\phi)]\}$ and so on.

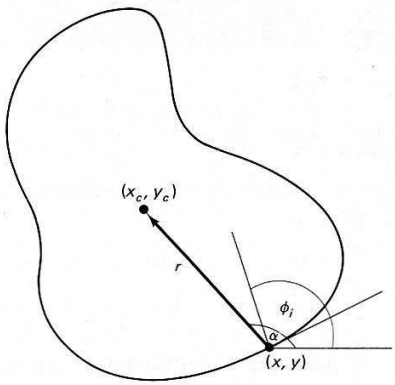

Fig. 4.8 Geometry used to form the R-Table.

Table 4.1

INCREMENTATION IN THE GENERALIZED HOUGH CASE

Angle measured from figure boundary to reference point	*Set of radii* $\{\mathbf{r}^k\}$ *where* $\mathbf{r} = (r, \alpha)$
ϕ_1	$\mathbf{r}_1^1, \mathbf{r}_2^1, \ldots, \mathbf{r}_{n_1}^1$
ϕ_2	$\mathbf{r}_1^2, \mathbf{r}_2^2, \ldots, \mathbf{r}_{n_2}^2$
.	.
.	.
.	.
ϕ_m	$\mathbf{r}_1^m, \mathbf{r}_2^m, \ldots, \mathbf{r}_{n_m}^m$

The generalized Hough algorithm may be described as follows:

Algorithm 4.3: Generalized Hough

Step 0. Make a table (like Table 4.1) for the shape to be located.

Step 1. Form an accumulator array of possible reference points $A(x_{c\min} : x_{c\max}, y_{c\min} : y_{c\max})$ initialized to zero.

Step 2. For each edge point do the following:

Step 2.1. Compute $\phi(\mathbf{x})$

Step 2.2a. Calculate the possible centers; that is, for each table entry for ϕ, compute

$$x_c := x + r\ \phi\ \cos[\alpha(\phi)]$$

$$y_c := y + r\ \phi\ \sin[\alpha(\phi)]$$

Step 2.2b. Increment the accumulator array

$$A(x_c, y_c) := A(x_c, y_c) + 1$$

Step 3. Possible locations for the shape are given by maxima in array A.

The results of using this transform to detect a shape are shown in Fig. 4.9. Figure 4.9a shows an image of shapes. The R-table has been made for the middle shape. Figure 4.9b shows the Hough transform for the shape, that is, $A(x_c, y_c)$ displayed as an image. Figure 4.9c shows the shape given by the maxima of

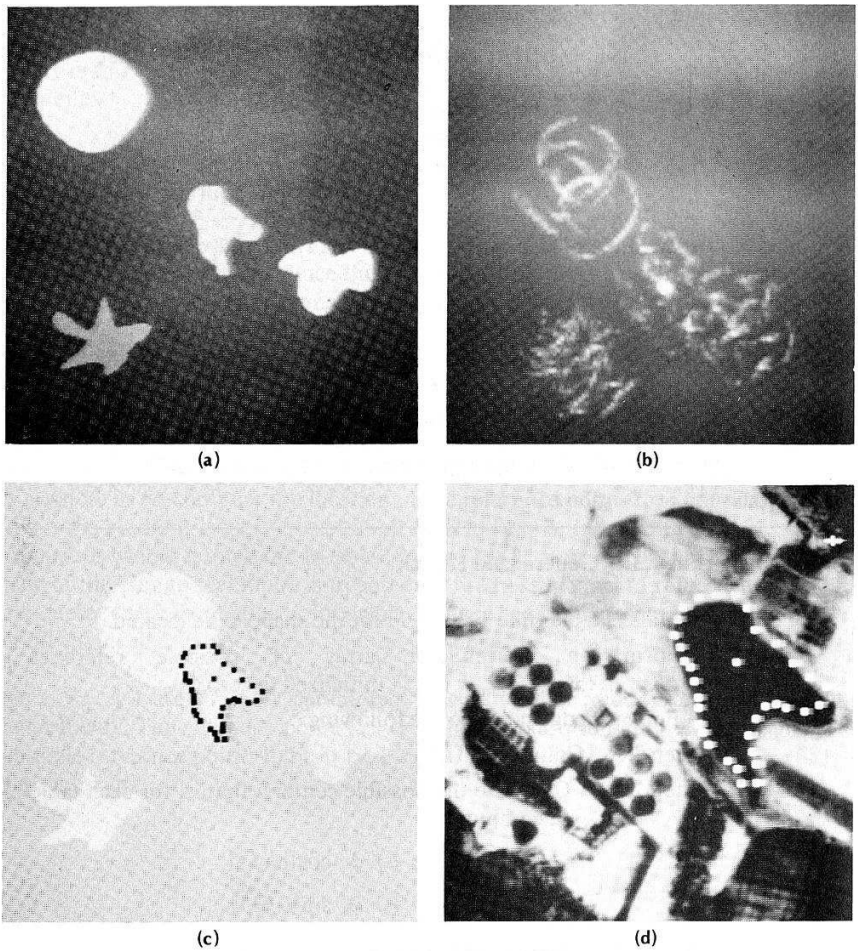

Fig. 4.9 Applying the Generalized Hough technique. (a) Synthetic image. (b) Hough Transform $A(x_c, y_c)$ for middle shape. (c) Detected shape. (d) Same shape in an aerial image setting.

$A(x_c, y_c)$ overlaid on top of the image. Finally, Fig. 4.9d shows the Hough transform used to detect a pond of the same shape in an aerial image.

What about the parameters of scale and rotation, S and θ? These are readily accommodated by expanding the accumulator array and doing more work in the incrementation step. Thus in step 1 the accumulator array is changed to

$$(x_{c\min} : x_{c\max}, y_{c\min} : y_{c\max}, S_{\min} : S_{\max}, \theta_{\min} : \theta_{\max})$$

and step 2.2a is changed to

for each table entry for ϕ do

for each S and θ

$$x_c := x + r(\phi) S \cos[\alpha(\phi) + \theta]$$

$$y_c := y + r(\phi) S \sin[\alpha(\phi) + \theta]$$

Finally, step 2.2b is now

$$A(x_c, y_c, S, \theta) := A(x_c, y_c, S, \theta) + 1$$

4.4 EDGE FOLLOWING AS GRAPH SEARCHING

A graph is a general object that consists of a set of nodes $\{n_i\}$ and arcs between nodes $< n_i, n_j >$. In this section we consider graphs whose arcs may have numerical weights or *costs* associated with them. The search for the boundary of an object is cast as a search for the lowest-cost path between two nodes of a weighted graph.

Assume that a gradient operator is applied to the gray-level image, creating the magnitude image $s(\mathbf{x})$ and direction image $\phi(\mathbf{x})$. Now interpret the elements of the direction image $\phi(\mathbf{x})$ as nodes in a graph, each with a weighting factor $s(\mathbf{x})$. Nodes $\mathbf{x}_i$, $\mathbf{x}_j$ have arcs between them if the contour directions $\phi(\mathbf{x}_i)$, $\phi(\mathbf{x}_j)$ are appropriately aligned with the arc directed in the same sense as the contour direction. Figure 4.10 shows the interpretation. To generate Fig. 4.10b impose the following restrictions. For an arc to connect from $\mathbf{x}_i$ to $\mathbf{x}_j$, $\mathbf{x}_j$ must be one of the three possible eight-neighbors in front of the contour direction $\phi(\mathbf{x}_i)$ and, furthermore, $g(\mathbf{x}_i)$

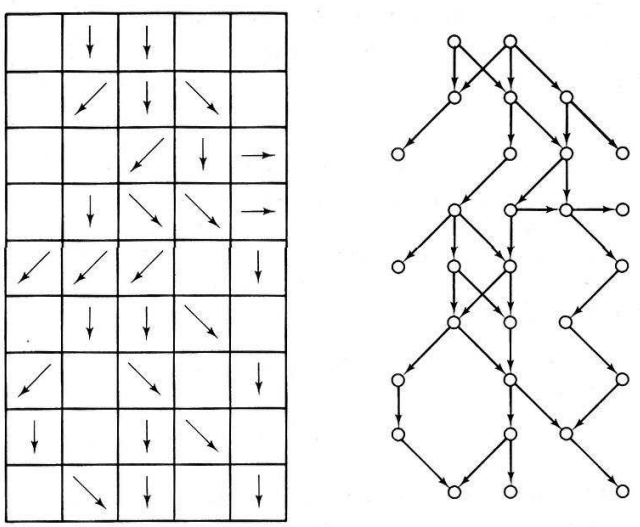

Fig. 4.10 Interpreting a gradient image as a graph (see text).

$> T$; $g(\mathbf{x}_j) > T$, where T is a chosen constant, and $|\{[\phi(\mathbf{x}_i) - \phi(\mathbf{x}_j)] \bmod 2\pi\}| < \pi/2$. (Any or all of these restrictions may be modified to suit the requirements of a particular problem.)

To generate a path in a graph from $\mathbf{x}_A$ to $\mathbf{x}_B$ one can apply the well-known technique of heuristic search [Nilsson 1971, 1980]. The specific use of heuristic search to follow edges in images was first proposed by [Martelli 1972]. Suppose:

1. That the path should follow contours that are directed from $\mathbf{x}_A$ to $\mathbf{x}_B$
2. That we have a method for generating the successor nodes of a given node (such as the heuristic described above)
3. That we have an evaluation function $f(\mathbf{x}_j)$ which is an estimate of the optimal cost path from $\mathbf{x}_A$ to $\mathbf{x}_B$ constrained to go through $\mathbf{x}_j$

Nilsson expresses $f(\mathbf{x}_i)$ as the sum of two components: $g(\mathbf{x}_i)$, the estimated cost of journeying from the *start node* $\mathbf{x}_A$ to $\mathbf{x}_i$, and $h(\mathbf{x}_i)$, the estimated cost of the path from $\mathbf{x}_i$ to $\mathbf{x}_B$, the *goal node.*

With the foregoing preliminaries, the heuristic search algorithm (called the A algorithm by Nilsson) can be stated as:

Algorithm 4.4: Heuristic Search (the A Algorithm)

1. "Expand" the start node (put the successors on a list called OPEN with pointers back to the start node).
2. Remove the node $\mathbf{x}_i$ of minimum f from OPEN. If $\mathbf{x}_i = \mathbf{x}_B$, then stop. Trace back through pointers to find optimal path. If OPEN is empty, fail.
3. Else expand node $\mathbf{x}_i$, putting successors on OPEN with pointers back to $\mathbf{x}_i$. Go to step 2.

The component $h(\mathbf{x}_i)$ plays an important role in the performance of the algorithm; if $h(\mathbf{x}_i) = 0$ for all i, the algorithm is a *minimum-cost search* as opposed to a *heuristic search.* If $h(\mathbf{x}_i) > h^*(\mathbf{x}_i)$ (the actual optimal cost), the algorithm may run faster, but may miss the minimum-cost path. If $h(\mathbf{x}_i) < h^*(\mathbf{x}_i)$, the search will always produce a minimum-cost path, provided that h also satisfies the following consistency condition:

> If for any two nodes $\mathbf{x}_i$ and $\mathbf{x}_j$, $k(\mathbf{x}_i, \mathbf{x}_j)$ is the minimum cost of getting from $\mathbf{x}_i$ to $\mathbf{x}_j$ (if possible), then
>
> $$k(\mathbf{x}_i, \mathbf{x}_j) \geqslant h^*(\mathbf{x}_i) - h^*(\mathbf{x}_j)$$

With our edge elements, there is no guarantee that a path can be found since there may be insurmountable gaps between $\mathbf{x}_A$ and $\mathbf{x}_B$. If finding the edge is crucial, steps should be taken to interpolate edge elements prior to the search, or gaps may be crossed by using the edge element definition of [Martelli 1972]. He defines

edges on the image grid structure so that an edge can have a direction even though there is no local gray-level change. This definition is depicted in Fig. 4.11a.

4.4.1 Good Evaluation Functions

A good evaluation function has components specific to the particular task as well as components that are relatively task-independent. The latter components are discussed here.

1. *Edge strength.* If edge strength is a factor, the cost of adding a particular edge element at $\mathbf{x}$ can be included as

$$M - s(\mathbf{x}) \qquad \text{where } M = \max_{\mathbf{x}} s(\mathbf{x})$$

2. *Curvature.* If low-curvature boundaries are desirable, curvature can be measured as some monotonically increasing function of

$$diff[\phi(\mathbf{x}_i) - \phi(\mathbf{x}_j)]$$

where diff measures the angle between the edge elements at $\mathbf{x}_j$ and $\mathbf{x}_i$.

3. *Proximity to an approximation.* If an approximate boundary is known, boundaries near this approximation can be favored by adding:

$$d = dist(\mathbf{x}_i, B)$$

to the cost measure. The dist operator measures the minimum distance of the new point $\mathbf{x}_i$ to the approximate boundary B.

4. *Estimates of the distance to the goal.* If the curve is reasonably linear, points near the goal may be favored by estimating h as $d(\mathbf{x}_i, \mathbf{x}_{goal})$, where d is a distance measure.

Specific implementations of these measures appear in [Ashkar and Modestino 1978; Lester et al. 1978].

4.4.2 Finding All the Boundaries

What if the objective is to find *all* boundaries in the image using heuristic search? In one system [Ramer 1975] Hueckel's operator (Chapter 3) is used to obtain

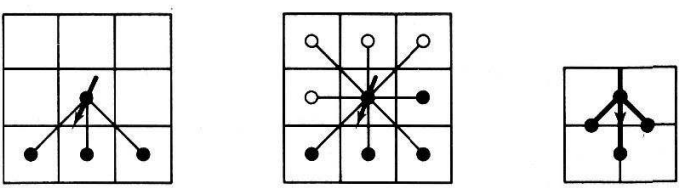

Fig. 4.11 Successor conventions in heuristic search (see text).

strokes, another name for the magnitude and direction of the local gray-level changes. Then these strokes are combined by heuristic search to form sequences of edge elements called *streaks*. Streaks are an intermediate organization which are used to assure a slightly broader coherence than is provided by the individual Hueckel edges. A bidirectional search is used with four eight-neighbors defined in front of the edge and four eight-neighbors behind the edge, as shown in Fig. 4.11b. The search algorithm is as follows:

1. Scan the stroke (edge) array for the most prominent edge.
2. Search in front of the edge until no more successors exist (i.e., a gap is encountered).
3. Search behind the edge until no more predecessors exist.
4. If the bidirectional search generates a path of 3 or more strokes, the path is a streak. Store it in a streak list and go to step 1.

Strokes that are part of a streak cannot be reused; they are marked when used and subsequently skipped.

There are other heuristic procedures for pruning the streaks to retain only *prime streaks*. These are shown in Fig. 4.12. They are essentially similar to the re-

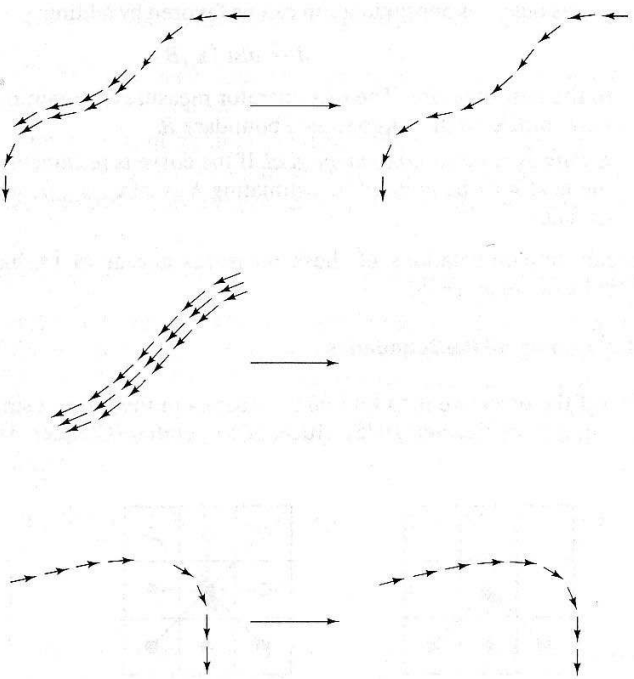

Fig. 4.12 Operations in the creation of prime streaks.

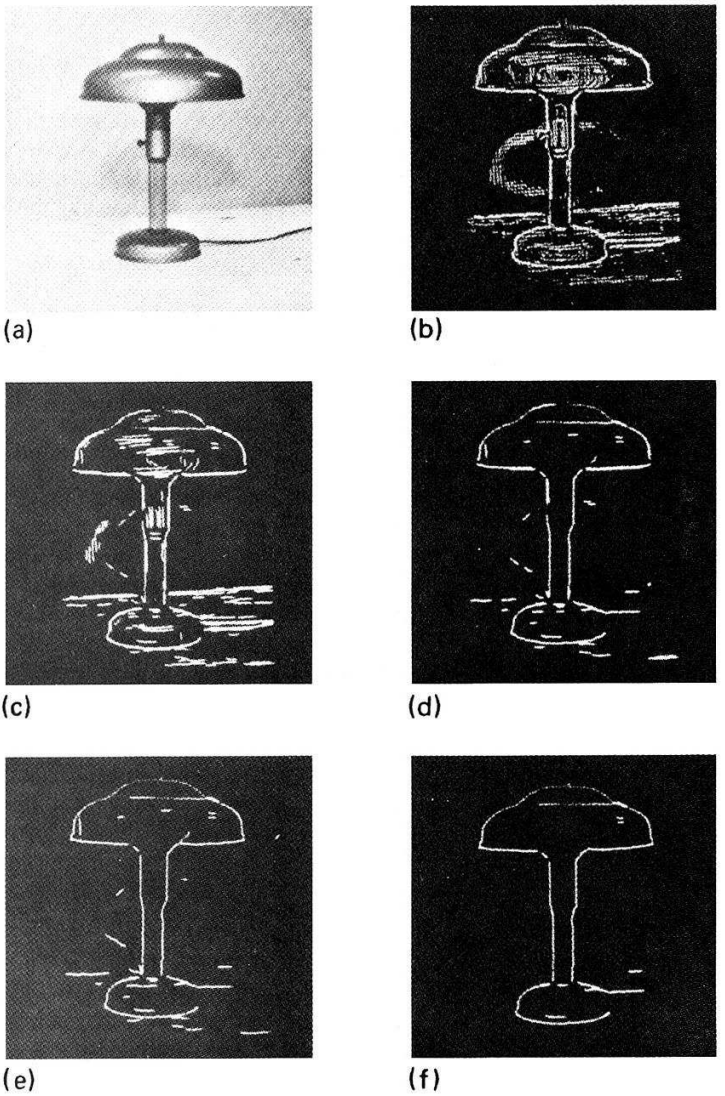

Fig. 4.13 Ramer's results.

laxation operations described in Section 3.3.5. The resultant streaks must still be analyzed to determine the objects they represent. Nevertheless, this method represents a cogent attempt to organize bottom-up edge following in an image. Fig. 4.13 shows an example of Ramer's technique.

4.4.3 Alternatives to the A Algorithm

The primary disadvantage with the heuristic search method is that the algorithm must keep track of a set of current best paths (nodes), and this set may become very large. These nodes represent tip nodes for the portion of the tree of possible paths that has been already examined. Also, since all the costs are nonnegative, a good path may eventually look expensive compared to tip nodes near the start node. Thus, paths from these newer nodes will be extended by the algorithm even though, from a practical standpoint, they are unlikely. Because of these disadvantages, other less rigorous search procedures have proven to be more practical, five of which are described below.

Pruning the Tree of Alternatives

At various points in the algorithm the tip nodes on the OPEN list can be pruned in some way. For example, paths that are short or have a high cost per unit length can be discriminated against. This pruning operation can be carried out whenever the number of alternative tip nodes exceeds some bound.

Modified Depth-First Search

Depth-first search is a meaningful concept if the search space is structured as a tree. Depth-first search means always evaluating the most recent expanded son. This type of search is performed if the OPEN list is structured as a stack in the A algorithm and the top node is always evaluated next. Modifications to this method use an evaluation function f to rate the successor nodes and expand the best of these. Practical examples can be seen in [Ballard and Sklansky 1976; Wechsler and Sklansky 1977; Persoon 1976].

Least Maximum Cost

In this elegant idea [Lester 1978], only the maximum-cost arc of each path is kept as an estimate of g. This is like finding a mountain pass at minimum altitude. The advantage is that g does not build up continuously with depth in the search tree, so that good paths may be followed for a long time. This technique has been applied to finding the boundaries of blood cells in optical microscope images. Some results are shown in Fig. 4.14.

Branch and Bound

The crux of this method is to have some upper bound on the cost of the path [Chien and Fu 1974]. This may be known beforehand or may be computed by actually generating a path between the desired end points. Also, the evaluation function must be monotonically increasing with the length of the path. With these conditions we start generating paths, excluding partial paths when they exceed the current bound.

Modified Heuristic Search

Sometimes an evaluation function that assigns negative costs leads to good results. Thus good paths keep getting better with respect to the evaluation function, avoiding the problem of having to look at all paths near the starting point.

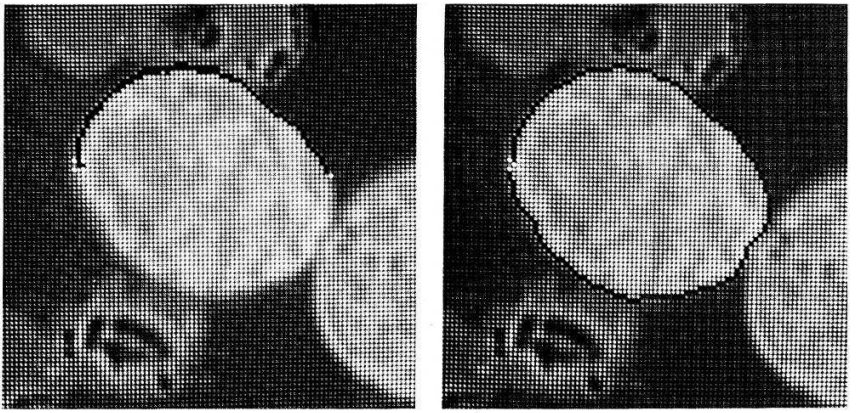

(a) (b)

Fig. 4.14 Using least maximum cost in heuristic search to find cell boundaries in microscope images. (a) A stage in the search process. (b) The completed boundary.

However, the price paid is the sacrifice of the mathematical guarantee of finding the least-cost path. This could be reflected in unsatisfactory boundaries. This method has been used in cineangiograms with satisfactory results [Ashkar and Modestino 1978].

4.5 EDGE FOLLOWING AS DYNAMIC PROGRAMMING

4.5.1 Dynamic Programming

Dynamic programming [Bellman and Dreyfus 1962] is a technique for solving optimization problems when not all variables in the evaluation function are interrelated simultaneously. Consider the problem

$$\max_{x_i} h(x_1, x_2, x_3, x_4) \tag{4.8}$$

If nothing is known about h, the only technique that guarantees a global maximum is exhaustive enumeration of all combinations of discrete values of $x_1, \ldots, x_4$. Suppose that

$$h(\cdot) = h_1(x_1, x_2) + h_2(x_2, x_3) + h_3(x_3, x_4) \tag{4.9}$$

x_1 only depends on x_2 in h_1. Maximize over x_1 in h_1 and tabulate the best value of $h_1(x_1, x_2)$ for each x_2:

$$f_1(x_2) = \max_{x_1} h_1(x_1, x_2) \tag{4.10}$$

Since the values of h_2 and h_3 do not depend on x_1, they need not be considered at

this point. Continue in this manner and eliminate x_2 by computing $f_2(x_3)$ as

$$f_2(x_3) = \max_{x_2}[f_1(x_2) + h_2(x_2, x_3)] \tag{4.11}$$

and

$$f_3(x_4) = \max_{x_3}[f_2(x_3) + h_3(x_3, x_4)] \tag{4.12}$$

so that finally

$$\max_{x_i} h = \max_{x_4} f_3(x_4) \tag{4.13}$$

Generalizing the example to N variables, where $f_0(x_1) = 0$,

$$f_{n-1}(x_n) = \max_{x_{n-1}}[f_{n-2}(x_{n-1}) + h_{n-1}(x_{n-1}, x_n)] \tag{4.14}$$

$$\max_{x_i} h(x_i, \ldots, x_N) = \max_{x_N} f_{N-1}(x_N)$$

If each x_i took on 20 discrete values, then to compute $f_N(x_{N+1})$ one must evaluate the maximand for 20 different combinations of x_N and x_{N+1}, so that the resultant computational effort involves $(N-1)20^2 + 20$ such evaluations. This is a striking improvement over exhaustive evaluation, which would involve 20^N evaluations of h!

Consider the artificial example summarized in Table 4.2. In this example, each $\mathbf{x}$ can take on one of three discrete values. The h_i are completely described by their respective tables. For example, the value of $h_i(0, 1) = 5$. The solution steps are summarized in Table 4.3. In step 1, for each x_2 the value of x_1 that maximizes $h_1(x_1, x_2)$ is computed. This is the largest entry in each of the columns of h. Store the function value as $f_1(x_2)$ and the optimizing value of x_1 also as a function of x_2. In step 2, add $f_1(x_2)$ to $h_2(x_2, x_3)$. This is done by adding f_1 to each row of h_2, thus computing the quantity inside the braces of (4.11). Now to complete step 2, for each x_3, compute the x_2 that maximizes $h_2 + f_1$ by selecting the largest entry in each row of the appropriate table. The rest of the steps are straightforward once these are understood. The solution is found by tracing back through the tables. For example, for $x_4 = 2$ we see that the best x_3 is -1, and therefore the best x_2 is 3 and x_1 is 1. This step is denoted by arrows.

Table 4.2

DEFINITION OF *h*

x_1 \ x_2	1	2	3
0	5	7	3
1	2	1	8
2	6	3	3

h_1

x_2 \ x_3	−1	0	1
1	1	7	1
2	1	1	3
3	5	6	2

h_2

x_3 \ x_4	1	2	3
−1	7	9	8
0	2	3	6
1	5	4	1

h_3

Table 4.3

METHOD OF SOLUTION USING DYNAMIC PROGRAMMING

Step 1

x_2	f_1	x_1
1	6	2
2	7	0
(3)	8	(1)

Step 2

x_2 \ x_3	−1	0	1
1	7	13	7
2	8	8	(10)
3	(13)	(14)	

x_3	f_2	x_2
(−1)	13	(3)
0	14	3
1	10	2

Step 3

x_3 \ x_4	1	2	3
−1	(20)	(22)	(21)
0	16	17	20
1	15	14	11

x_4	f_3	x_3
1	20	−1
(2)	(22)	(−1)
3	21	−1

Step 4: Optimal x_i's are found by examing tables (dashed line shows the order in which they are recovered).

Solution: $h^* = 22$
$x_1^* = 1, x_2^* = 3, x_3^* = -1, x_4^* = 2$

4.5.2 Dynamic Programming for Images

To formulate the boundary-following procedure as dynamic programming, one must define an evaluation function that embodies a notion of the "best boundary" [Montanari 1971; Ballard 1976]. Suppose that a local edge detection operator is ap-

plied to a gray-level picture to produce edge magnitude and direction information. Then one possible criterion for a "good boundary" is a weighted sum of high cumulative edge strength and low cumulative curvature; that is, for an n-segment curve,

$$h(\mathbf{x}_1, \ldots, \mathbf{x}_n) = \sum_{k=1}^{n} s(\mathbf{x}_k) + \alpha \sum_{k=1}^{n-1} q(\mathbf{x}_k, \mathbf{x}_{k+1}) \tag{4.16}$$

where the implicit constraint is that consecutive $\mathbf{x}_k$'s must be grid neighbors:

$$\|\mathbf{x}_k - \mathbf{x}_{k+1}\| \leqslant \sqrt{2} \tag{4.17}$$

$$q(\mathbf{x}_k, \mathbf{x}_{k+1}) = diff\,[\phi(\mathbf{x}_k), \phi(\mathbf{x}_{k+1})] \tag{4.18}$$

where α is negative. The function g we take to be edge strength, i.e., $g(x) = s(x)$. Notice that this evaluation function is in the form of (4.9) and can be optimized in stages:

$$f_0(\mathbf{x}_1) \equiv 0 \tag{4.19}$$

$$f_1(\mathbf{x}_2) = \max_{x_1} [s(\mathbf{x}_1) + \alpha q(\mathbf{x}_1, \mathbf{x}_2) + f_0(\mathbf{x}_1)] \tag{4.20}$$

$$f_k(\mathbf{x}_{k+1}) = \max_{x_k} [s(\mathbf{x}_k) + \alpha q(\mathbf{x}_k, \mathbf{x}_{k+1}) + f_{k-1}(\mathbf{x}_k)] \tag{4.21}$$

These equations can be put into the following steps:

Algorithm 4.5: Dynamic Programming for Edge Finding

1. Set $k = 1$.
2. Consider only $\mathbf{x}$ such that $s(\mathbf{x}) \geqslant T$. For each of these $\mathbf{x}$, define low-curvature pixels "in front of" the contour direction.
3. Each of these pixels may have a curve emanating from it. For $k = 1$, the curve is one pixel in length. Join the curve to $\mathbf{x}$ that optimizes the left-hand side of the recursion equation.
4. If $k = N$, pick the best f_{N-1} and stop. Otherwise, set $k = k + 1$ and go to step 2.

This algorithm can be generalized to the case of picking a *curve* emanating from $\mathbf{x}$ (that we have already generated): Find the end of that curve, and join the best of three curves emanating from the end of that curve. Figure 4.15 shows this process. The equations for the general case are

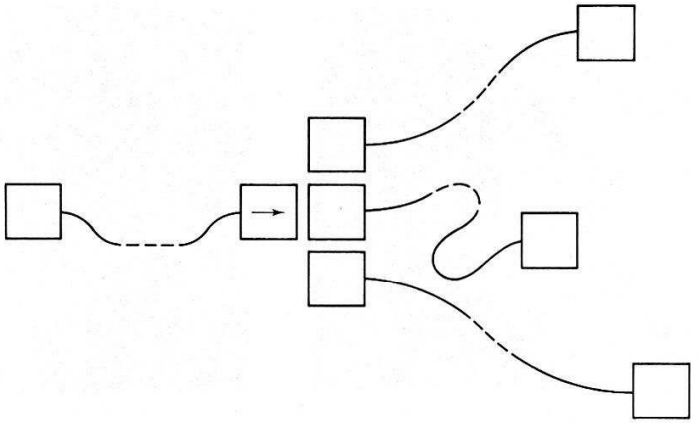

Fig. 4.15 DP optimization for boundary tracing.

$$f_0(\mathbf{x}_1) \equiv 0$$

$$f_l(\mathbf{x}_{k+1}) = \max_{x_k}[s(\mathbf{x}_k) + \alpha q(\mathbf{x}_k, t(\mathbf{x}_{k+1})) + f_{l-1}(\mathbf{x}_k)] \tag{4.22}$$

where the curve length n is related to α by a building sequence $n(l)$ such that $n(1) = 1$, $n(L) = N$, and $n(l) - n(l-1)$ is a member of $\{n(k) | k = 1, \ldots, l-1\}$. Also, $t(\mathbf{x}_k)$ is a function that extracts the tail pixel of the curve headed by $\mathbf{x}_k$. Further details may be found in [Ballard 1976].

Results from the area of tumor detection in radiographs give a sense of this method's performance. Here it is known that the boundary inscribes an approximately circular tumor, so that circular cues can be used to assist the search. In Fig. 4.16, (a) shows the image containing the tumor, (b) shows the cues, and (c) shows the boundary found by dynamic programming overlaid on the image.

Another application of dynamic programming may be found in the pseudo-parallel road finder of Barrow [Barrow 1976].

4.5.3 Lower Resolution Evaluation Functions

In the dynamic programming formulation just developed, the components $g(\mathbf{x}_k)$ and $q(\mathbf{x}_k, \mathbf{x}_{k+1})$ in the evaluation function are very localized; the variables $\mathbf{x}$ for successive s and q are in fact constrained to be grid neighbors. This need not be the case: The $\mathbf{x}$ can be very distant from each other without altering the basic technique. Furthermore, the functions g and q need not be local gradient and absolute curvature, respectively, but can be any functions defined on permissible $\mathbf{x}$. This general formulation of the problem for images was first described by [Fischler and

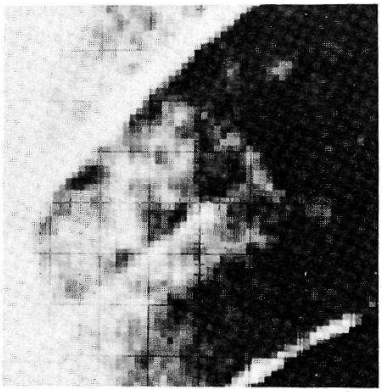

(a)

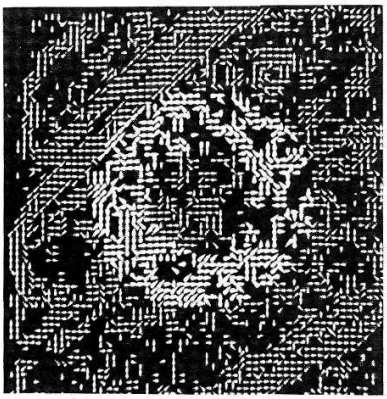

(b)

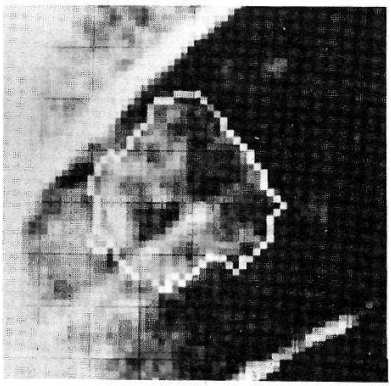

(c)

Fig. 4.16 Results of DP in boundary tracing. (a) Image containing tumor. (b) Contour cues. (c) Resultant boundary.

Elschlager 1973]. The Fischler and Elschlager formulation models an object as a set of parts and relations between parts, represented as a graph. Template functions, denoted by $g(\mathbf{x})$, measure how well a part of the model matches a part of the image at the point $\mathbf{x}$. (These local functions may be defined in any manner whatsoever.) "Relational functions," denoted by $q_{kj}(\mathbf{x}, \mathbf{y})$, measure how well the position of the match of the kth part at $(\mathbf{x})$ agrees with the position of the match of the jth part at $(\mathbf{y})$.

The basic notions are shown by a technique simplified from [Chien and Fu 1974] to find the boundaries of lungs in chest films. The lung boundaries are modeled with a polygonal approximation defined by the five key points. These points are the top of the lung, the two clavicle-lung junctions, and the two lower corners. To locate these points, local functions $g(\mathbf{x}_k)$ are defined which should be maximized when the corresponding point $\mathbf{x}_k$ is correctly determined. Similarly, $q(\mathbf{x}_k, \mathbf{x}_j)$ is a function relating points $\mathbf{x}_k$ and $\mathbf{x}_j$. In their case, Chien and Fu used the following functions:

$$T(\mathbf{x}) \equiv \text{template centered at } \mathbf{x} \text{ computed as an aggregate of a set of chest radiographs}$$

$$g(\mathbf{x}_k) = \sum_{\mathbf{x}} \frac{T(\mathbf{x} - \mathbf{x}_k) f(\mathbf{x})}{|T||f|}$$

and

$$\theta(\mathbf{x}_k, \mathbf{x}_j) = \text{expected angular orientation of } \mathbf{x}_k \text{ from } \mathbf{x}_j$$

$$q(\mathbf{x}_k \mathbf{x}_j) = \left[\theta(\mathbf{x}_k, \mathbf{x}_j) - \arctan \frac{y_k - y_j}{x_k - x_j} \right]$$

With this formulation no further modifications are necessary and the solution may be obtained by solving Eqs. (4.19) through (4.21), as before. For purposes of comparison, this method was formalized using a lower-resolution objective function. Figure 4.17 shows Chien and Fu's results using this method with five template functions.

4.5.4 Theoretical Questions about Dynamic Programming

The Interaction Graph

This graph describes the interdependence of variables in the objective function. In the examples the interaction graph was simple: Each variable depended on only two others, resulting in the graph of Fig. 4.18a. A more complicated case is the one in 4.18b, which describes an objective function of the following form:

$$h(\,) = h_1(x_1, x_2) + h_2(x_2, x_3, x_4) + h_3(x_3, x_4, x_5, x_6)$$

For these cases the dynamic programming technique still applies, but the computational effort increases exponentially with the number of interdependencies. For example, to eliminate x_2 in h_2, all possible combinations of x_3 and x_4 must be considered. To eliminate x_3 in h_3, all possible combinations of x_4, x_5, and x_6, and so forth.

Dynamic Programming versus Heuristic Search

It has been shown [Martelli 1976] that for finding a path in a graph between two points, which is an abstraction of the work we are doing here, heuristic search methods can be more efficient than dynamic programming methods. However, the point to remember about dynamic programming is that it efficiently builds paths from multiple starting points. If this is required by a particular task, then dynamic programming would be the method of choice, unless a very powerful heuristic were available.

4.6 CONTOUR FOLLOWING

If nothing is known about the boundary shape, but regions have been found in the image, the boundary is recovered by one of the simplest edge-following operations: "blob finding" in images. The ideas are easiest to present for binary images:

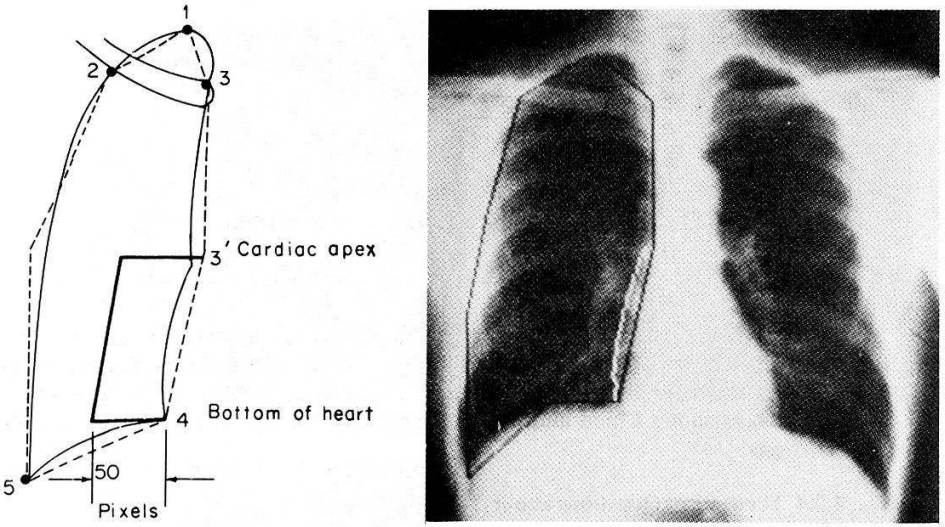

Fig. 4.17 Results of using local templates and global relations. (a) Model. (b) Results.

Given a binary image, the goal is find the boundaries of all distinct regions in the image.

This can be done simply by a procedure that functions like Papert's turtle [Papert 1973; Duda and Hart 1973]:

1. Scan the image until a region pixel is encountered.
2. If it is a region pixel, turn left and step; else, turn right and step.
3. Terminate upon return to the starting pixel.

Figure 4.19 shows the path traced out by the procedure. This procedure requires the region to be four-connected for a consistent boundary. Parts of an eight-connected region can be missed. Also, some bookkeeping is necessary to generate an exact sequence of boundary pixels without duplications.

A slightly more elaborate algorithm due to [Rosenfeld 1968] generates the boundary pixels exactly. It works by first finding a four-connected background pixel from a known boundary pixel. The next boundary pixel is the first pixel encountered when the eight neighbors are examined in a counter clockwise order from the background pixel. Many details have to be introduced into algorithms that follow contours of irregular eight-connected figures. A good exposition of these is given in [Rosenfeld and Kak 1976].

4.6.1 Extension to Gray-Level Images

The main idea behind contour following is to start with a point that is believed to be on the boundary and to keep extending the boundary by adding points in the contour directions. The details of these operations vary from task to task. The gen-

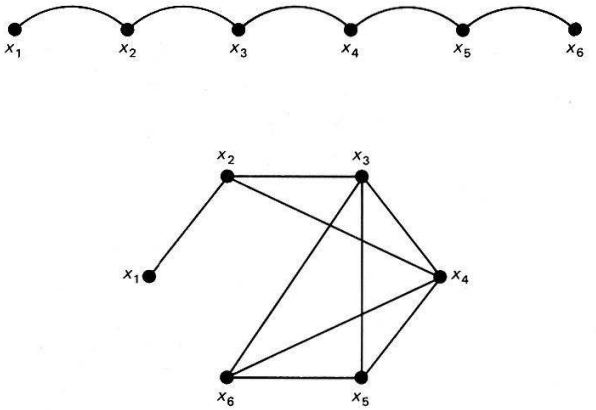

Fig. 4.18 Interaction graphs for DP (see text).

eralization of the contour follower to gray-level images uses local gradients with a magnitude $s(\mathbf{x})$ and direction $\phi(\mathbf{x})$ associated with each point $\mathbf{x}$. ϕ points in the direction of maximum change. If $\mathbf{x}$ is on the boundary of an image object, neighboring points on the boundary should be in the general direction of the contour directions, $\phi(\mathbf{x}) \pm \pi/2$, as shown by Fig. 4.20. A representative procedure is adapted from [Martelli 1976]:

1. Assume that an edge has been detected up to a point $\mathbf{x}_i$. Move to the point $\mathbf{x}_j$ adjacent to $\mathbf{x}_i$ in the direction perpendicular to the gradient of $\mathbf{x}_i$. Apply the gradient operator to $\mathbf{x}_j$; if its magnitude is greater than (some) threshold, this point is added to the edge.
2. Otherwise, compute the average gray level of the 3×3 array centered on $\mathbf{x}_j$, compare it with a suitably chosen threshold, and determine whether $\mathbf{x}_j$ is inside or outside the object.
3. Make another attempt with a point $\mathbf{x}_k$ adjacent to $\mathbf{x}_i$ in the direction perpendicular to the gradient at $\mathbf{x}_i$ plus or minus $(\pi/4)$, according to the outcome of the previous test.

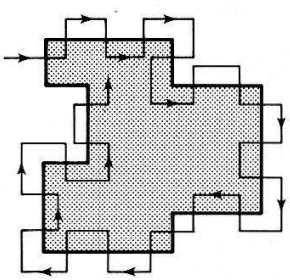

Fig. 4.19 Finding the boundary in a binary image.

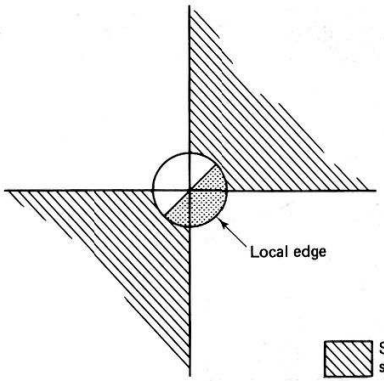

Fig. 4.20 Angular orientations for contour following.

4.6.2 Generalization to Higher-Dimensional Image Data

The generalization of contour following to higher-dimensional spaces is straightforward [Liu 1977; Herman and Liu 1978]. The search involved is, in fact, slightly more complex than contour following and is more like the graph searching methods described in Section 4.4. Higher-dimensional image spaces arise when the image has more than two spatial dimensions, is time-varying, or both. In these images the notion of a gradient is the same (a vector describing the maximum gray-level change and its corresponding direction), but the intuitive interpretation of the corresponding edge element may be difficult. In three dimensions, edge elements are primitive surface elements, separating volumes of differing gray level. The objective of contour following is to link together neighboring surface elements with high gradient modulus values and similar orientations into larger boundaries. In four dimensions, "edge elements" are primitive volumes; contour following links neighboring volumes with similar gradients.

The contour following approach works well when there is little noise present and no "spurious" boundaries. Unfortunately, if either of these conditions is present, the contour-following algorithms are generally unsatisfactory; they are easily thwarted by gaps in the data produced by noise, and readily follow spurious boundaries. The methods described earlier in this chapter attempt to overcome these difficulties through more elaborate models of the boundary structure.

EXERCISES

4.1 Specify a heuristic search algorithm that will work with "crack" edges such as those in Fig. 3.12.

4.2 Describe a modification of Algorithm 4.2 to detect parabolae in gray-level images.

4.3 Suppose that a relation $h(x_1, x_6)$ is added to the model described by Fig. 4.18a so that now the interaction graph is cyclical. Show formally how this changes the optimization steps described by Eqs. (4.11) through (4.13).

4.4 Show formally that the Hough technique without gradient direction information is equivalent to template matching (Chapter 3).

4.5 Extend the Hough technique for ellipses described by Eqs. (4.7a) through (4.7d) to ellipses oriented at an arbitrary angle θ to the x axis.

4.6 Show how to use the generalized Hough technique to detect hexagons.

REFERENCES

ASHKAR, G. P. and J. W. MODESTINO. "The contour extraction problem with biomedical applications." *CGIP 7*, 1978, 331–355.

BALLARD, D. H. *Hierarchic detection of tumors in chest radiographs.* Basel: Birkhäuser-Verlag (ISR-16), January 1976.

BALLARD, D. H. "Generalizing the Hough transform to detect arbitrary shapes." *Pattern Recognition 13*, 2, 1981, 111–122.

BALLARD, D. H. and J. SKLANSKY. "A ladder-structured decision tree for recognizing tumors in chest radiographs." *IEEE Trans. Computers 25*, 1976, 503-513.

BALLARD, D. H., M. MARINUCCI, F. PROIETTI-ORLANDI, A. ROSSI-MARI, and L. TENTARI. "Automatic analysis of human haemoglobin fingerprints." *Proc.*, 3rd Meeting, International Society of Haemotology, London, August 1975.

BARROW, H. G. "Interactive aids for cartography and photo interpretation." Semi-Annual Technical Report, AI Center, SRI International, December 1976.

BELLMAN, R. and S. DREYFUS. *Applied Dynamic Programming.* Princeton, NJ: Princeton University Press, 1962.

BOLLES, R. "Verification vision for programmable assembly." *Proc.*, 5th IJCAI, August 1977, 569-575.

CHIEN, Y. P. and K. S. FU. "A decision function method for boundary detection." *CGIP 3*, 2, June 1974, 125-140.

DUDA, R. O. and P. E. HART. "Use of the Hough transformation to detect lines and curves in pictures." *Commun. ACM 15*, 1, January 1972, 11–15.

DUDA, R. O. and P. E. HART. *Pattern Recognition and Scene Analysis.* New York: Wiley, 1973.

FISCHLER, M. A. and R. A. ELSCHLAGER. "The representation and matching of pictoral patterns." *IEEE Trans. Computers 22*, January 1973.

HERMAN, G. T. and H. K. LIU. "Dynamic boundary surface detection." *CGIP 7*, 1978, 130-138.

HOUGH, P. V. C. "Method and means for recognizing complex patterns." U.S. Patent 3,069,654; 1962.

KELLY, M.D. "Edge detection by computer using planning." In *MI6*, 1971.

KIMME, C., D. BALLARD, and J. SKLANSKY. "Finding circles by an array of accumulators." *Commun. ACM 18*, 2, 1975, 120-122.

LANTZ, K. A., C. M. BROWN and D. H. BALLARD. "Model-driven vision using procedure decription: motivation and application to photointerpretation and medical diagnosis." *Proc.*, 22nd International Symp., Society of Photo-optical Instrumentation Engineers, San Diego, CA, August 1978.

LESTER, J. M., H. A. WILLIAMS, B. A. WEINTRAUB, and J. F. BRENNER, "Two graph searching techniques for boundary finding in white blood cell images." *Computers in Biology and Medicine 8*, 1978, 293-308.

LIU, H. K. "Two- and three-dimensional boundary detection." *CGIP 6*, 2, April 1977, 123-134.

MARR, D. "Analyzing natural images; a computational theory of texture vision." Technical Report 334, AI Lab, MIT, June 1975.

MARTELLI, A. "Edge detection using heuristic search methods." *CGIP 1*, 2, August 1972, 169-182.

MARTELLI, A. "An application of heuristic search methods to edge and contour detection." *Commun. ACM 19*, 2, February 1976, 73–83.

MONTANARI, U. "On the optimal detection of curves in noisy pictures." *Commun. ACM 14*, 5, May 1971, 335-345.

NILSSON, N. J. *Problem-Solving Methods in Artificial Intelligence.* New York: McGraw-Hill, 1971.

NILSSON, N. J. *Principles of Artificial Intelligence.* Palo Alto, CA: Tioga, 1980.

PAPERT, S. "Uses of technology to enhance education." Technical Report 298, AI Lab, MIT, 1973.

PERSOON, E. "A new edge detection algorithm and its applications in picture processing." *CGIP 5*, 4, December 1976, 425-446.

RAMER, U. "Extraction of line structures from photographs of curved objects." *CGIP 4*, 2, June 1975, 81-103.

ROSENFELD, A. *Picture Processing by Computer.* New York: Academic Press, 1968.

ROSENFELD, A. and A. C. KAK. *Digital Picture Processing.* New York: Academic Press, 1976.

SELFRIDGE, P. G., J. M. S. PREWITT, C. R. DYER, and S. RANADE. "Segmentation algorithms for abdominal computerized tomography scans." *Proc.*, 3rd COMPSAC, November 1979, 571-577.

WECHSLER, H. and J. SKLANSKY. "Finding the rib cage in chest radiographs." *Pattern Recognition 9*, 1977, 21-30.

Region Growing 5

5.1 REGIONS

Chapter 4 concentrated on the linear features (discontinuities of image gray level) that often correspond to object boundaries, interesting surface detail, and so on. The "dual" problem to finding edges around regions of differing gray level is to find the regions themselves. The goal of region growing is to use image characteristics to map individual pixels in an input image to sets of pixels called *regions.* An image region might correspond to a world object or a meaningful part of one.

Of course, very simple procedures will derive a boundary from a connected region of pixels, and conversely can fill a boundary to obtain a region. There are several reasons why both region growing and line finding survive as basic segmentation techniques despite their redundant-seeming nature. Although perfect regions and boundaries are interconvertible, the processing to find them initially differs in character and applicability; besides, perfect edges or regions are not always required for an application. Region-finding and line-finding techniques can cooperate to produce a more reliable segmentation.

The geometric characteristics of regions depend on the domain. Usually, they are considered to be connected two-dimensional areas. Whether regions can be disconnected, non-simply connected (have holes), should have smooth boundaries, and so forth depends on the region-growing technique and the goals of the work. Ultimately, it is often the segmentation goal to partition the entire image into quasi-disjoint regions. That is, regions have no two-dimensional overlaps, and no pixel belongs to the interior of more than one region. However, there is no single definition of region—they may be allowed to overlap, the whole image may not be partitioned, and so forth.

Our discussion of region growers will begin with the most simple kinds and progress to the more complex. The most primitive region growers use only aggregates of properties of local groups of pixels to determine regions. More sophisti-

cated techniques "grow" regions by *merging* more primitive regions. To do this in a structured way requires sophisticated representations of the regions and boundaries. Also, the merging *decisions* can be complex, and can depend on descriptions of the boundary structure separating regions in addition to the region semantics. A good survey of early techniques is [Zucker 1976].

The techniques we consider are:

1. *Local techniques.* Pixels are placed in a region on the basis of their properties or the properties of their close neighbors.
2. *Global techniques.* Pixels are grouped into regions on the basis of the properties of large numbers of pixels distributed throughout the image.
3. *Splitting and merging techniques.* The foregoing techniques are related to individual pixels or sets of pixels. State space techniques merge or split regions using graph structures to represent the regions and boundaries. Both local and global merging and splitting criteria can be used.

The effectiveness of region growing algorithms depends heavily on the application area and input image. If the image is sufficiently simple, say a dark blob on a light background, simple local techniques can be surprisingly effective. However, on very difficult scenes, such as outdoor scenes, even the most sophisticated techniques still may not produce a satisfactory segmentation. In this event, region growing is sometimes used conservatively to preprocess the image for more knowledgeable processes [Hanson and Riseman 1978].

In discussing the specific algorithms, the following definitions will be helpful. Regions R_k are considered to be sets of points with the following properties:

$\mathbf{x}_i$ in a region R is *connected* to $\mathbf{x}_j$ iff there is a sequence $\{\mathbf{x}_i, \ldots, \mathbf{x}_j\}$ such that $\mathbf{x}_k$ and $\mathbf{x}_{k+1}$ are connected and all the points are in R. (5.1)

R is a *connected region* if the set of points $\mathbf{x}$ in R has the property that every pair of points is connected. (5.2)

$$I, \text{ the entire image} = \bigcup_{k=1}^{m} R_k \tag{5.3}$$

$$R_i \bigcap R_j = \phi, \qquad i \neq j \tag{5.4}$$

A set of regions satisfying (5.2) through (5.4) is known as a *partition.* In segmentation algorithms, each region often is a unique, homogeneous area. That is, for some Boolean function $H(R)$ that measures region homogeneity,

$$H(R_k) = \text{true for all } k \tag{5.5}$$

$$H(R_i \bigcup R_j) = \text{false for } i \neq j \tag{5.6}$$

Note that R_i does not have to be connected. A weaker but still useful criterion is that neighboring regions not be homogeneous.

5.2 A LOCAL TECHNIQUE: BLOB COLORING

The counterpart to the edge tracker for binary images is the blob-coloring algorithm. Given a binary image containing four-connected blobs of 1's on a background of 0's, the objective is to "color each blob"; that is, assign each blob a different label. To do this, scan the image from left to right and top to bottom with a special L-shaped template shown in Fig. 5.1. The coloring algorithm is as follows.

Algorithm 5.1: Blob Coloring

Let the initial color, $k = 1$. Scan the image from left to right and top to bottom.

If $f(\mathbf{x}_C) = 0$ then continue
else
begin

if $(f(\mathbf{x}_U) = 1$ and $f(\mathbf{x}_L) = 0)$
then color $(\mathbf{x}_C) :=$ color $(\mathbf{x}_U)$

if $(f(\mathbf{x}_L) = 1$ and $f(\mathbf{x}_U) = 0)$
then color $(\mathbf{x}_C) :=$ color $(\mathbf{x}_L)$

if $(f(\mathbf{x}_L) = 1$ and $f(\mathbf{x}_U) = 1)$
then begin
color $(\mathbf{x}_C) :=$ color $(\mathbf{x}_L)$
color $(\mathbf{x}_L)$ is equivalent to color $(\mathbf{x}_U)$
end

comment: two colors are equivalent.

if $(f(\mathbf{x}_L) = 0$ and $f(\mathbf{x}_U) = 0)$
then color $(\mathbf{x}_L) := k$; $k := k + 1$

comment: new color

end

After one complete scan of the image the color equivalences can be used to assure that each object has only one color. This binary image algorithm can be used as a simple region-grower for gray-level images with the following modifications. If in a

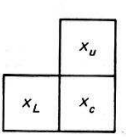

Fig. 5.1 L-shaped template for blob coloring.

gray-level image $f(\mathbf{x}_C)$ is approximately equal to $f(\mathbf{x}_U)$, assign $\mathbf{x}_C$ to the same region (blob) as $\mathbf{x}_U$. This is equivalent to the condition $f(\mathbf{x}_C) = f(\mathbf{x}_U) = 1$ in Algorithm 5.1. The modifications to the steps in the algorithm are straightforward.

5.3 GLOBAL TECHNIQUES: REGION GROWING VIA THRESHOLDING

This approach assumes an object-background image and picks a threshold that divides the image pixels into either object or background:

$\mathbf{x}$ is part of the Object iff $f(\mathbf{x}) > T$
Otherwise it is part of the Background

The best way to pick the threshold T is to search the histogram of gray levels, assuming it is bimodal, and find the minimum separating the two peaks, as in Fig. 5.2. Finding the right valley between the peaks of a histogram can be difficult when the histogram is not a smooth function. Smoothing the histogram can help but does not guarantee that the correct minimum can be found. An elegant method for treating bimodal images assumes that the histogram is the sum of two composite normal functions and determines the valley location from the normal parameters [Chow and Kaneko 1972].

The single-threshold method is useful in simple situations, but primitive. For example, the region pixels may not be connected, and further processing such as that described in Chapter 2 may be necessary to smooth region boundaries and remove noise. A common problem with this technique occurs when the image has a background of varying gray level, or when collections we would like to call regions vary smoothly in gray level by more than the threshold. Two modifications of the threshold approach to ameliorate the difficulty are: (1) high-pass filter the image to deemphasize the low-frequency background variation and then try the original technique; and (2) use a spatially varying threshold method such as that of [Chow and Kaneko 1972].

The Chow-Kaneko technique divides the image up into rectangular subimages and computes a threshold for each subimage. A subimage can fail to have a threshold if its gray-level histogram is not bimodal. Such subimages receive inter-

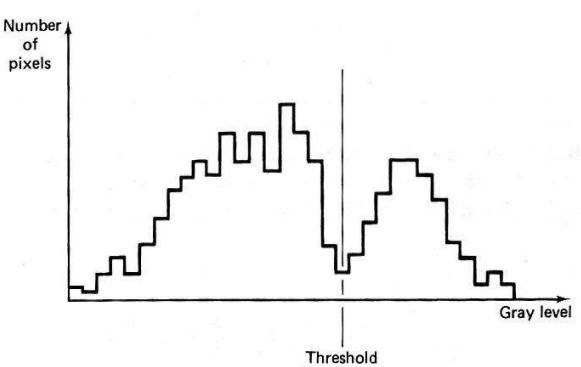

Fig. 5.2 Threshold determination from gray-level histogram.

polated thresholds from neighboring subimages that are bimodal, and finally the entire picture is thresholded by using the separate thresholds for each subimage.

5.3.1 Thresholding in Multidimensional Space

An interesting variation to the basic thresholding paradigm uses color images; the basic digital picture function is vector-valued with red, blue, and green components. This vector is augmented with possibly nonlinear combinations of these values so that the augmented picture vector has a number of components. The idea is to re-represent the color solid redundantly and hope to find color parameters for which thresholding does the desired segmentation. One implementation of this idea used the red, green, and blue color components; the intensity, saturation, and hue components; and the N.T.S.C. Y, I, Q components (Chapter 2) [Ohlander et al. 1979].

The idea of thresholding the components of a picture vector is used in a primitive form for multispectral LANDSAT imagery [Robertson et al. 1973]. The novel extension in this algorithm is the recursive application of this technique to nonrectangular subregions.

The region partitioning is then as follows:

Algorithm 5.2: Region Growing via Recursive Splitting

1. Consider the entire image as a region and compute histograms for each of the picture vector components.
2. Apply a peak-finding test to each histogram. If at least one component passes the test, pick the component with the most significant peak and determine two thresholds, one either side of the peak (Fig. 5.3). Use these thresholds to divide the region into subregions.
3. Each subregion may have a "noisy" boundary, so the binary representation of the image achieved by thresholding is smoothed so that only a single connected subregion remains. For binary smoothing see ch. 8 and [Rosenfeld and Kak 1976].
4. Repeat steps 1 through 3 for each subregion until no new subregions are created (no histograms have significant peaks).

A refinement of step 2 of this scheme is to create histograms in higher-dimensional space [Hanson and Riseman 1978]. Multiple regions are often in the same histogram peak when a single measurement is used. The advantage of the multimeasurement histograms is that these different regions are often separated into individual peaks, and hence the segmentation is improved. Figure 5.4 shows some results using a three-dimensional RGB color space.

The figure shows the clear separation of peaks in the three-dimensional histogram that is not evident in either of the one-dimensional histograms. How many

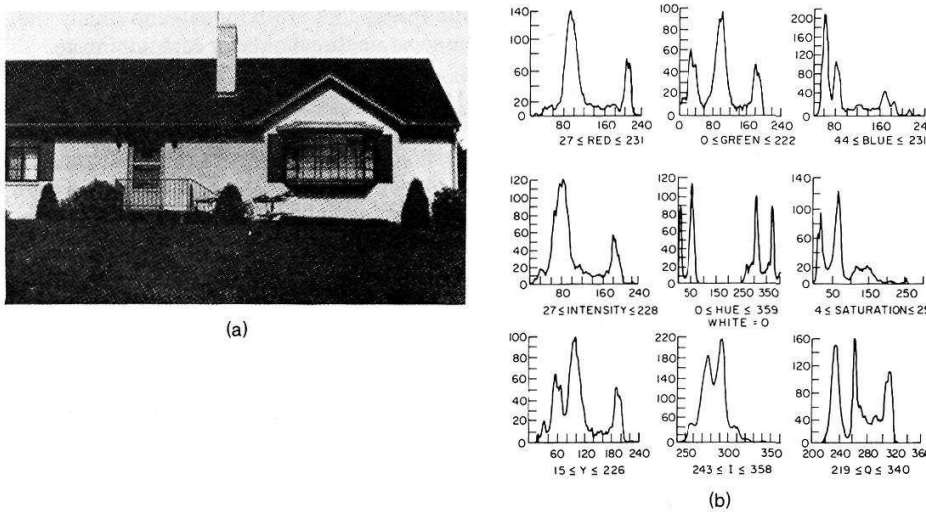

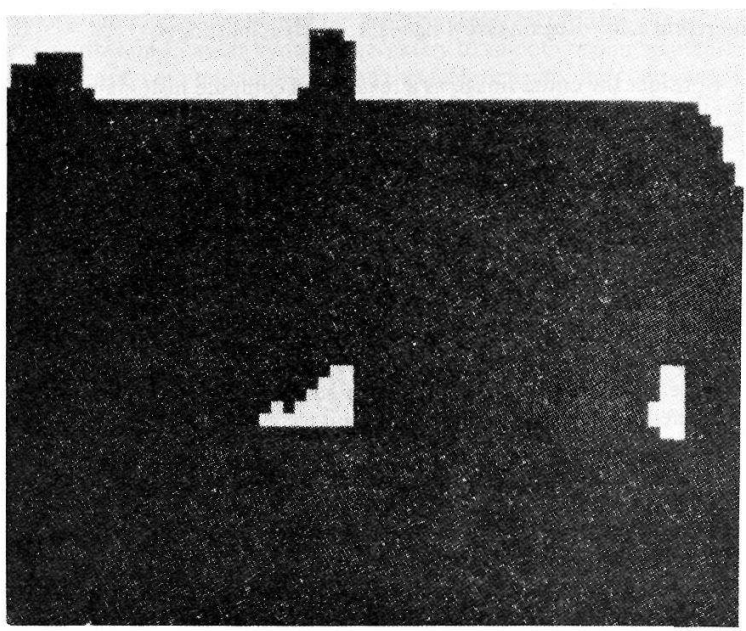

Fig. 5.3 Peak detection and threshold determination. (a) Original image. (b) Histograms. (c) Image segments resulting from first histogram peak.

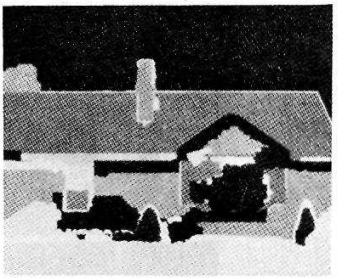

(d)

Fig. 5.3 (d) Final segments.

dimensions should be used? Obviously, there is a trade-off here: As the dimensionality becomes larger, the discrimination improves, but the histograms are more expensive to compute and noise effects may be more pronounced.

5.3.2 Hierarchical Refinement

This technique uses a pyramidal image representation (Section 3.7) [Harlow and Eisenbeis 1973]. Region growing is applied to a coarse resolution image. When the algorithm has terminated at one resolution level, the pixels near the boundaries of regions are disassociated with their regions. The region-growing process is then repeated for just these pixels at a higher-resolution level. Figure 5.5 shows this structure.

5.4 SPLITTING AND MERGING

Given a set of regions R_k, $k = 1,\ldots,m$, a low-level segmentation might require the basic properties described in Section 5.1 to hold. The important properties from the standpoint of segmentation are Eqs. (5.5) and (5.6).

If Eq. (5.5) is not satisfied for some k, it means that that region is inhomogeneous and should be split into subregions. If Eq. (5.6) is not satisfied for some i and j, then regions i and j are collectively homogeneous and should be merged into a single region.

In our previous discussions we used

$$H(R) = \begin{cases} \text{true} & \text{if all neighboring pairs of points} \\ & \text{in } R \text{ are such that } f(\mathbf{x}) - f(\mathbf{y}) < T \\ \text{false} & \text{otherwise} \end{cases} \tag{5.7}$$

and

$$H(R) = \begin{cases} \text{true} & \text{if the points in } R \text{ pass a} \\ & \text{bimodality or peak test} \\ \text{false} & \text{otherwise} \end{cases} \tag{5.8}$$

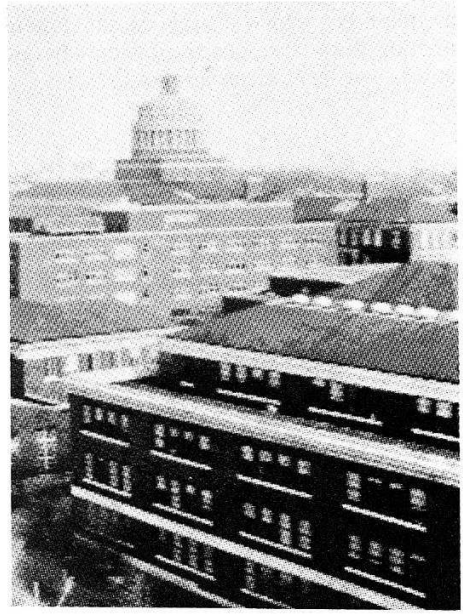

(a)

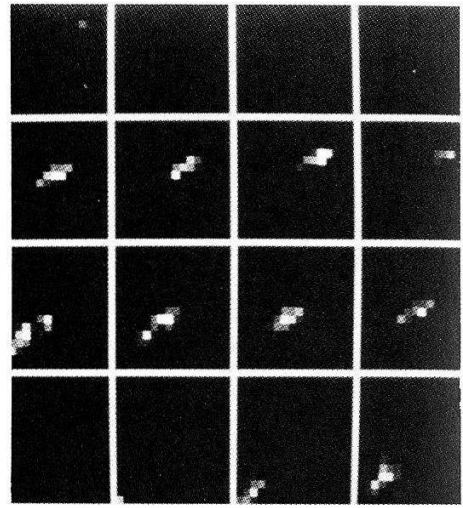

(b)

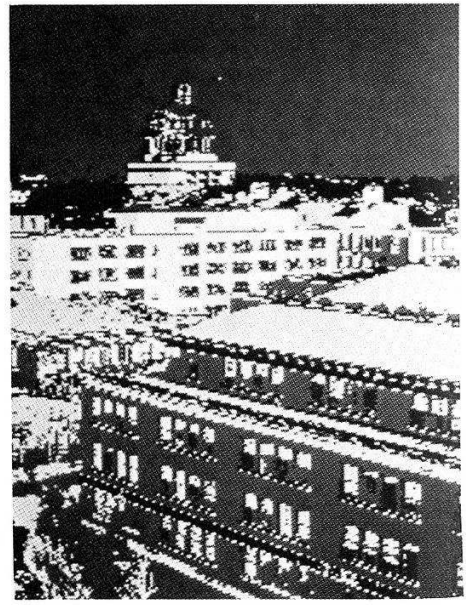

(c)

Fig. 5.4 Multi-dimensional histograms in segmentation. (a) Image. (b) RGB histogram showing successive planes through a 16 × 16 × 16 color space. (c) Segments. (See color inserts.)

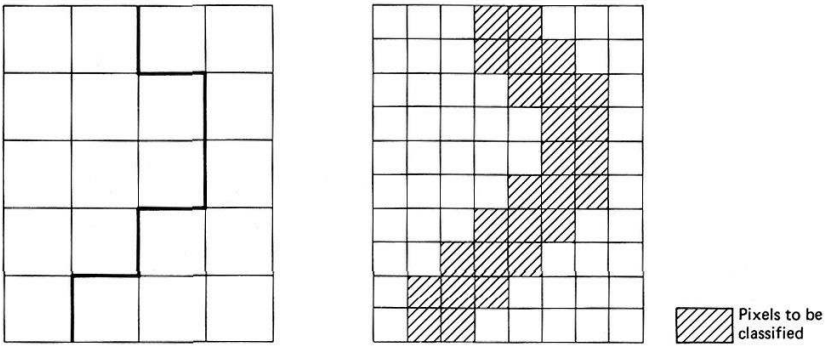

Fig. 5.5 Hierarchical region refinement.

A way of working toward the satisfaction of these homogeneity criteria is the split-and-merge algorithm [Horowitz and Pavlidis 1974]. To use the algorithm it is necessary to organize the image pixels into a pyramidal grid structure of regions. In this grid structure, regions are organized into groups of four. Any region can be split into four subregions (except a region consisting of only one pixel), and the appropriate groups of four can be merged into a single larger region. This structure is incorporated into the following region-growing algorithm.

Algorithm 5.3: Region Growing via Split and Merge [Horowitz and Pavlidis 1974]

1. Pick any grid structure, and homogeneity property H. If for any region R in that structure, $H(R) =$ false, split that region into four subregions. If for any four appropriate regions $R_{k1}, \ldots, R_{k4}$, $H(R_{k1} \bigcup R_{k2} \bigcup R_{k3} \bigcup R_{k4}) =$ true, merge them into a single region. When no regions can be further split or merged, stop.
2. If there are any neighboring regions R_i and R_j (perhaps of different sizes) such that $H(R_i \bigcup R_j) =$ true, merge these regions.

5.4.1 State-Space Approach to Region Growing

The "classical" state-space approach of artificial intelligence [Nilsson 1971, 1980] was first applied to region growing in [Brice and Fennema 1970] and significantly extended in [Feldman and Yakimovsky 1974]. This approach regards the initial two-dimensional image as a discrete state, where every sample point is a separate region. Changes of state occur when a boundary between regions is either removed or inserted. The problem then becomes one of searching allowable changes in state to find the best partition.

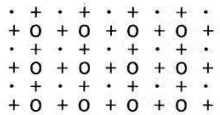

· Unassigned
+ Edge data
O Grey level data

Fig. 5.6 Grid structure for region representation [Brice and Fennema 1970].

An important part of the state-space approach is the use of data structures to allow regions and boundaries to be manipulated as units. This moves away from earlier techniques, which labeled each individual pixel according to its region. The high-level data structures do away with this expensive practice by representing regions with their boundaries and then keeping track of what happens to these boundaries during split-and merge-operations.

5.4.2 Low-level Boundary Data Structures

A useful representation for boundaries allows the splitting and merging of regions to proceed in a simple manner [Brice and Fennema 1970]. This representation introduces the notion of a supergrid S to the image grid G. These grids are shown in Fig. 5.6, where · and + correspond to supergrid and O to the subgrid. The representation is assumed to be four-connected (i.e., $\mathbf{x}1$ is a neighbor of $\mathbf{x}2$ if $\|\mathbf{x}1 - \mathbf{x}2\| \leqslant 1$).

With this notation boundaries of regions are directed crack edges (see Sec. 3.1) at the points marked +. That is, if point $\mathbf{x}_k$ is a neighbor of $\mathbf{x}_j$ and $\mathbf{x}_k$ is in a different region than $\mathbf{x}_j$, insert two edges for the boundaries of the regions containing $\mathbf{x}_j$ and $\mathbf{x}_k$ at the point + separating them, such that each edge traverses its associated region in a counterclockwise sense. This makes merge operations very simple: To merge regions R_k and R_l, remove edges of the opposite sense from the boundary as shown in Fig. 5.7a. Similarly, to split a region along a line, insert edges of the opposite sense in nearby points, as shown in Fig. 5.7b.

The method of [Brice and Fennema 1970] uses three criteria for merging regions, reflecting a transition from local measurements to global measurements. These criteria use measures of boundary strength s_{ij} and w_{ij} defined as

$$s_{ij} = |f(\mathbf{x}_i) - f(\mathbf{x}_j)| \tag{5.9}$$

$$w_k = \begin{cases} 1 & \text{if } s_k < T_1 \\ 0 & \text{otherwise} \end{cases} \tag{5.10}$$

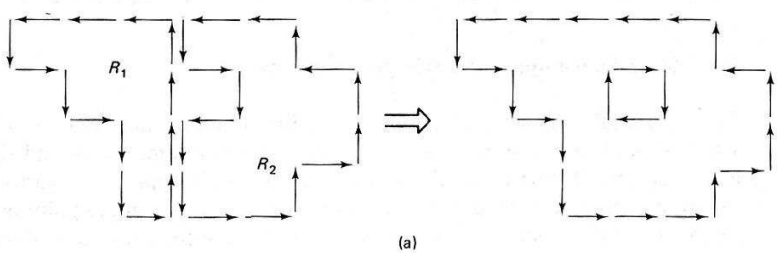

Fig. 5.7 Region operations on the grid structure of Fig. 5.6.

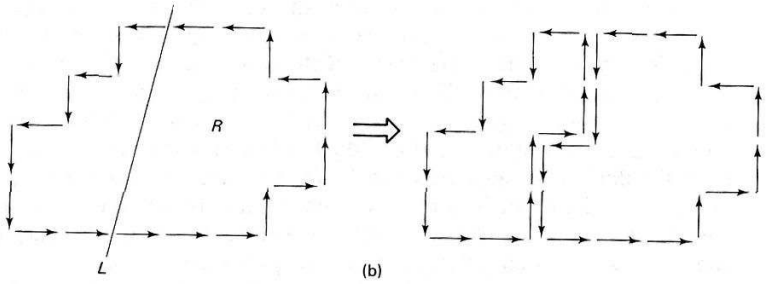

Fig. 5.7 (cont.)

where $\mathbf{x}_i$ and $\mathbf{x}_j$ are assumed to be on either side of a crack edge (Chapter 3). The three criteria are applied sequentially in the following algorithm:

Algorithm 5.4: Region Growing via Boundary Melting (T_k, $k = 1, 2, 3$ are preset thresholds)

1. For all neighboring pairs of points, remove the boundary between $\mathbf{x}_i$ and $\mathbf{x}_j$ if $i \neq j$ and $w_{ij} = 1$. When no more boundaries can be removed, go to step 2.
2. Remove the boundary between R_i and R_j if

$$\frac{W}{\min [p_i, p_j]} \geqslant T_2 \tag{5.11}$$

   where W is the sum of the w_{ij} on the common boundary between R_i and R_j, that have perimeters p_i and p_j respectively. When no more boundaries can be removed, go to step 3.
3. Remove the boundary between R_i and R_j if

$$W \geqslant T_3 \tag{5.12}$$

5.4.3 Graph-Oriented Region Structures

The Brice–Fennema data structure stores boundaries explicitly but does not provide for explicit representation of regions. This is a drawback when regions must be referred to as units. An adjunct scheme of region representation can be developed using graph theory. This scheme represents both regions and their boundaries explicitly, and this facilitates the storing and indexing of their semantic properties.

The scheme is based on a special graph called the *region adjacency graph*, and its "dual graph." In the region adjacency graph, nodes are regions and arcs exist between neighboring regions. This scheme is useful as a way of keeping track of regions, even when they are inscribed on arbitrary nonplanar surfaces (Chapter 9).

Consider the regions of an image shown in Fig. 5.8a. The region adjacency graph has a node in each region and an arc crossing each separate boundary segment. To allow a uniform treatment of these structures, define an artificial region that surrounds the image. This node is shown in Fig. 5.8b. For regions on a plane, the region adjacency graph is *planar* (can lie in a plane with no arcs intersecting) and its edges are undirected. The "dual" of this graph is also of interest. To constuct the dual of the adjacency graph, simply place nodes in each separate region and connect them with arcs wherever the regions are separated by an arc in the adjacency graph. Figure 5.8c shows that the dual of the region adjacency graph is like the original region boundary map; in Fig. 5.8b each arc may be associated with a specific boundary segment and each node with a junction between three or more boundary segments. By maintaining both the region adjacency graph and its dual, one can merge regions using the following algorithm:

Algorithm 5.5: Merging Using the Region-Adjacency Graph and Its Dual

Task: Merge neighboring regions R_i and R_j.

Phase 1. Update the region-adjacency graph.

1. Place edges between R_i and all neighboring regions of R_j (excluding, of course, R_i) that do not already have edges between themselves and R_i.
2. Delete R_j and all its associated edges.

Phase 2. Take care of the dual.

1. Delete the edges in the dual corresponding to the borders between R_i and R_j.
2. For each of the nodes associated with these edges:
   (a) if the resultant degree of the node is less than or equal to 2, delete the node and join the two dangling edges into a single edge.
   (b) otherwise, update the labels of the edges that were associated with j to reflect the new region label i.

Figure 5.9 shows these operations.

5.5 INCORPORATION OF SEMANTICS

Up to this point in our treatment of region growers, domain-dependent "semantics" has not explicitly appeared. In other words, region-merging decisions were based on raw image data and rather weak heuristics of general applicability about the likely shape of boundaries. As in early processing, the use of domain-dependent knowledge can affect region finding. Possible interpretations of regions can affect the splitting and merging process. For example, in an outdoor scene possible region interpretations might be sky, grass, or car. This kind of knowledge is quite separate from but related to measurable region properties such as intensity

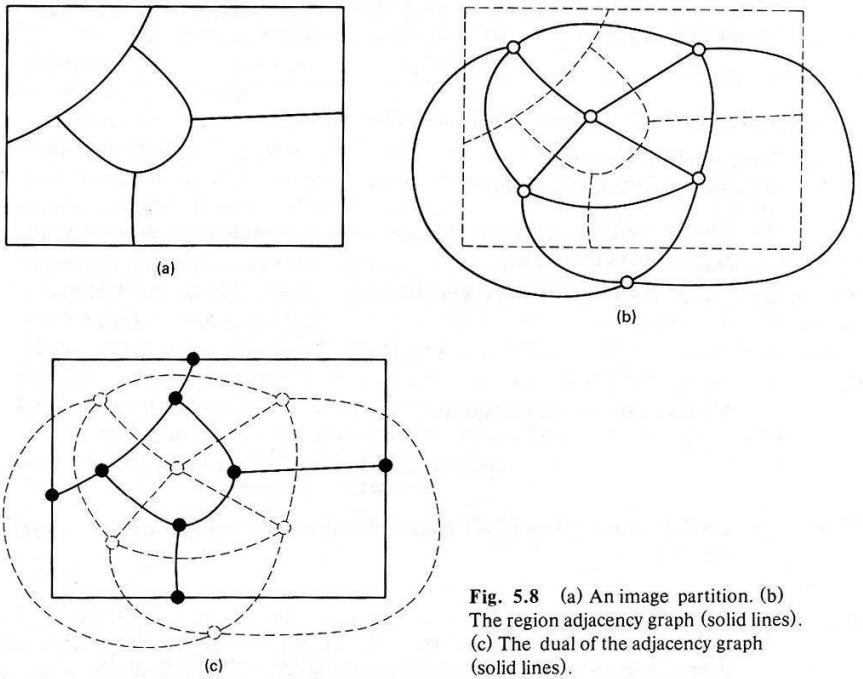

Fig. 5.8 (a) An image partition. (b) The region adjacency graph (solid lines). (c) The dual of the adjacency graph (solid lines).

and hue. An example shows how semantic labels for regions can guide the merging process. This approach was originally developed in [Feldman and Yakimovsky 1974]. it has found application in several complex vision systems [Barrow and Tenenbaum 1977; Hanson and Riseman 1978].

Early steps in the Feldman–Yakimovsky region grower used essentially the same steps as Brice–Fennema. Once regions attain significant size, semantic cri-

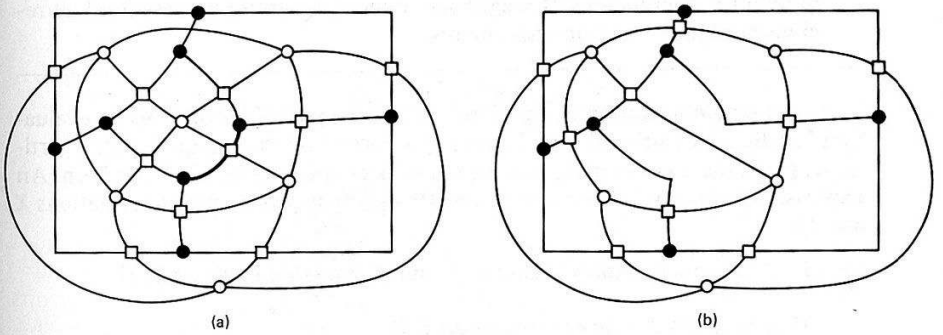

Fig. 5.9 Merging operations using the region adjacency graph and its dual. (a) Before merging regions separated by dark boundary line. (b) After merging.

teria are used. The region growing consists of four steps, as summed up in the following algorithm:

Algorithm 5.6 Semantic Region Growing

Nonsemantic Criteria
T_1 and T_2 are preset thresholds

1. Merge regions i, j as long as they have one weak separating edge until no two regions pass this test.
2. Merge regions i, j where $S(i, j) \leqslant T_2$ where

$$S(i, j) = \frac{c_1 + \alpha_{ij}}{c_2 + \alpha_{ij}}$$

where c_1 and c_2 are constants,

$$\alpha ij = \frac{(\text{area}_i)^{1/2} + (\text{area}_j)^{1/2}}{\text{perimeter}_i \cdot \text{perimeter}_j}$$

until no two regions pass this test. (This is a similar criterion to Algorithm 5.4, step 2.)

Semantic Criteria

3. Let B_{ij} be the boundary between R_i and R_j. Evaluate each B_{ij} with a Bayesian decision function that measures the (conditional) probability that B_{ij} separates two regions R_i and R_j of the *same interpretation*. Merge R_i and R_j if this conditional probability is less than some threshold. Repeat step 3 until no regions pass the threshold test.
4. Evaluate the interpretation of each region R_i with a Bayesian decision function that measures the (conditional) probability that an interpretation is the correct one for that region. Assign the interpretation to the region with the highest confidence of correct interpretation. Update the conditional probabilities for different interpretations of neighbors. Repeat the entire process until all regions have interpretation assignments.

The semantic portion of algorithm 5.6 had the goal of maximizing an evaluation function measuring the probability of a correct interpretation (labeled partition), given the measurements on the boundaries and regions of the partition. An expression for the evaluation function is (for a given partition and interpretations X and Y):

$$\max_{X, Y} \prod_{i, j} \{P[B_{ij} \text{ is a boundary between } X \text{ and } Y \mid \text{measurements on } B_{ij}]\}$$
$$\times \prod_i \{P[R_i \text{ is an } X \mid \text{measurements on } R_i]\}$$
$$\times \prod_i \{P[R_j \text{ is an } Y \mid \text{measurements on } R_j]\}$$

where P stands for probability and Π is the product operator.

How are these terms to be computed? Ideally, each conditional probability function should be known to a reasonable degree of accuracy; then the terms can be obtained by lookup.

However, the straightforward computation and representation of the conditional probability functions requires a massive amount of work and storage. An approximation used in [Feldman and Yakimovsky 1974] is to quantize the measurements and represent them in terms of a classification tree. The conditional probabilities can then be computed from data at the leaves of the tree. Figure 5.10 shows a hypothetical tree for the region measurements of intensity and hue, and interpretations ROAD, SKY, and CAR. Figure 5.11 shows the equivalent tree for two boundary measurements m and n and the same interpretations. These two figures indicate that $P[R_i \text{ is a CAR} \mid 0 \leqslant i < I, 0 \leqslant h < H_1] =$, and $P[B_{ij}$ divides two car regions $\mid M_k \leqslant m < M_{k+1}, N_l < n \leqslant N_{l+1} =$. These trees were created by laborious trials with correct segmentations of test images.

Now, finally, consider again step 3 of Algorithm 5.6. The probability that a boundary B_{ij} between regions R_i and R_j is false is given by

$$P_{\text{false}} = \frac{P_f}{P_t + P_f} \tag{5.13}$$

where

$$P_f = \sum \{P[B_{ij} \text{ is between two subregions } X \mid B_{ij}\text{'s measurements}]\} \tag{5.14a}$$
$$\times \{P[R_i \text{ is } X \mid \text{meas}]\} \times \{P[R_j \text{ is } X \mid \text{meas}]\}$$

$$P_t = \sum_{X,Y} \{P[B_{ij} \text{ is between } X \text{ and } Y \mid \text{meas}]\} \tag{5.14b}$$
$$\times \{P[R_i \text{ is } X \mid \text{meas}]\} \times \{P[R_j \text{ is } Y \mid \text{meas}]\}$$

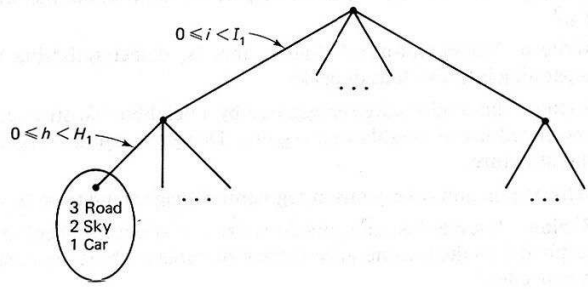

Fig. 5.10 Hypothetical classification tree for region measurements showing a particular branch for specific ranges of intensity and hue.

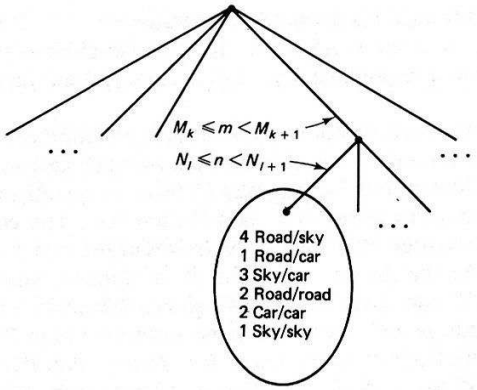

Fig. 5.11 Hypothetical classification tree for boundary measurements showing a specific branch for specific ranges of two measurements m and n.

And for step 4 of the algorithm,

$$\text{Confidence}_i = \frac{P[R_i \text{ is } X1 \mid \text{meas}]}{P[R_i \text{ is } X2 \mid \text{meas}]} \tag{5.15}$$

where $X1$, $X2$ are the first and second most likely interpretations, respectively. After the region is assigned interpretation $X1$, the neighbors are updated using

$$P[R_i \text{ is } X \mid \text{meas}] := Prob\ [Rj \text{ is } X \mid \text{meas}] \times P[B_{ij} \text{ is between } X \text{ and } X1 \mid \text{meas}] \tag{5.16}$$

EXERCISES

5.1 In Algorithm 5.1, show how one can handle the case where colors are equivalent. Do you need more than one pass over the image?

5.2 Show for the heuristic of Eq. (5.11) that

(a) $IT_2 \geq WT_2 > P_j$

(b) $P_m < P_i + I(1/T_2 - 2)$

where P_m is the perimeter of $R_i \bigcup R_j$, I is the perimeter common to both i and j and $P_m = \min(P_i, P_j)$. What does part (b) imply about the relation between T_2 and P_m?

5.3 Write a "histogram-peak" finder; that is, detect satisfying valleys in histograms separating intuitive hills or peaks.

5.4 Suppose that regions are represented by a neighbor list structure. Each region has an associated list of neighboring regions. Design a region-merging algorithm based on this structure.

5.5 Why do junctions of regions in segmented images tend to be trihedral?

5.6 Regions, boundaries, and junctions are the structures behind the region-adjacency graph and its dual. Generalize these structures to three dimensions. Is another structure needed?

5.7 Generalize the graph of Figure 5.8 to three dimensions and develop the merging algorithm analogous to Algorithm 5.5. (Hint: see Exercise 5.6.)

REFERENCES

BARROW, H. G. and J. M. TENENBAUM. "Experiments in model-driven scene segmentation." *Artificial Intelligence 8*, 3, June 1977, 241–274.

BRICE, C. and C. FENNEMA. "Scene analysis using regions." *Artificial Intelligence 1*, 3, Fall 1970, 205–226.

CHOW, C. K. and T. KANEKO. "Automatic boundary detection of the left ventricle from cineangiograms." *Computers and Biomedical Research 5*, 4, August 1972, 388–410.

FELDMAN, J. A. and Y. YAKIMOVSKY. "Decision theory and artificial intelligence: I. A semantics-based region analyzer." *Artificial Intelligence 5*, 4, 1974, 349–371.

HANSON, A. R. and E. M. RISEMAN. "Segmentation of natural scenes." In *CVS*, 1978.

HARLOW, C. A. and S. A. EISENBEIS. "The analysis of radiographic images." *IEEE Trans. Computers 22*, 1973, 678–688.

HOROWITZ, S. L. and T. PAVLIDIS. "Picture segmentation by a directed split-and-merge procedure." *Proc.*, 2nd IJCPR, August 1974, 424–433.

NILSSON, N. J. *Principles of Artificial Intelligence.* Palo Alto, CA: Tioga, 1980.

NILSSON, N. J. *Problem-Solving Methods in Artificial Intelligence.* New York: McGraw-Hill, 1971.

OHLANDER, R., K. PRICE, and D. R. REDDY. "Picture segmentation using a recursive region splitting method." *CGIP 8*, 3, December 1979.

ROBERTSON, T. V., P. H. SWAIN, and K. S. FU. "Multispectral image partitioning." TR-EE 73-26 (LARS Information Note 071373), School of Electrical Engineering, Purdue Univ., August 1973.

ROSENFELD, A. and A. C. KAK. *Digital Picture Processing.* New York: Academic Press, 1976.

ZUCKER, S. W. "Region growing: Childhood and adolescence." *CGIP 5*, 3, September 1976, 382–399.

Texture 6

6.1 WHAT IS TEXTURE?

The notion of texture admits to no rigid description, but a dictionary definition of texture as "something composed of closely interwoven elements" is fairly apt. The description of interwoven elements is intimately tied to the idea of texture resolution, which one might think of as the average amount of pixels for each discernable texture element. If this number is large, we can attempt to describe the individual elements in some detail. However, as this number nears unity it becomes increasingly difficult to characterize these elements individually and they merge into less distinct spatial patterns. To see this variability, we examine some textures.

Figure 6.1 shows "cane," "paper," "coffee beans," "brickwall," "coins," and "wire braid" after Brodatz's well-known book [Brodatz 1966]. Five of these examples are high-resolution textures: they show repeated primitive elements that exhibit some kind of variation. "Coffee beans," "brick wall" and "coins" all have obvious primitives (even if it is not so obvious how to extract these from image data). Two more examples further illustrate that one sometimes has to be creative in defining primitives. In "cane" the easiest primitives to deal with seem to be the physical holes in the texture, whereas in "wire braid" it might be better to model the physical relations of a loose weave of metallic wires. However, the paper texture does not fit nicely into this mold. This is not to say that there are not possibilities for primitive elements. One is regions of lightness and darkness formed by the ridges in the paper. A second possibility is to use the reflectance models described in Section 3.5 to compute "pits" and "bumps." However, the elements seem to be "just beyond our perceptual resolving power" [Laws 1980], or in our terms, the elements are very close in size to individual pixels.

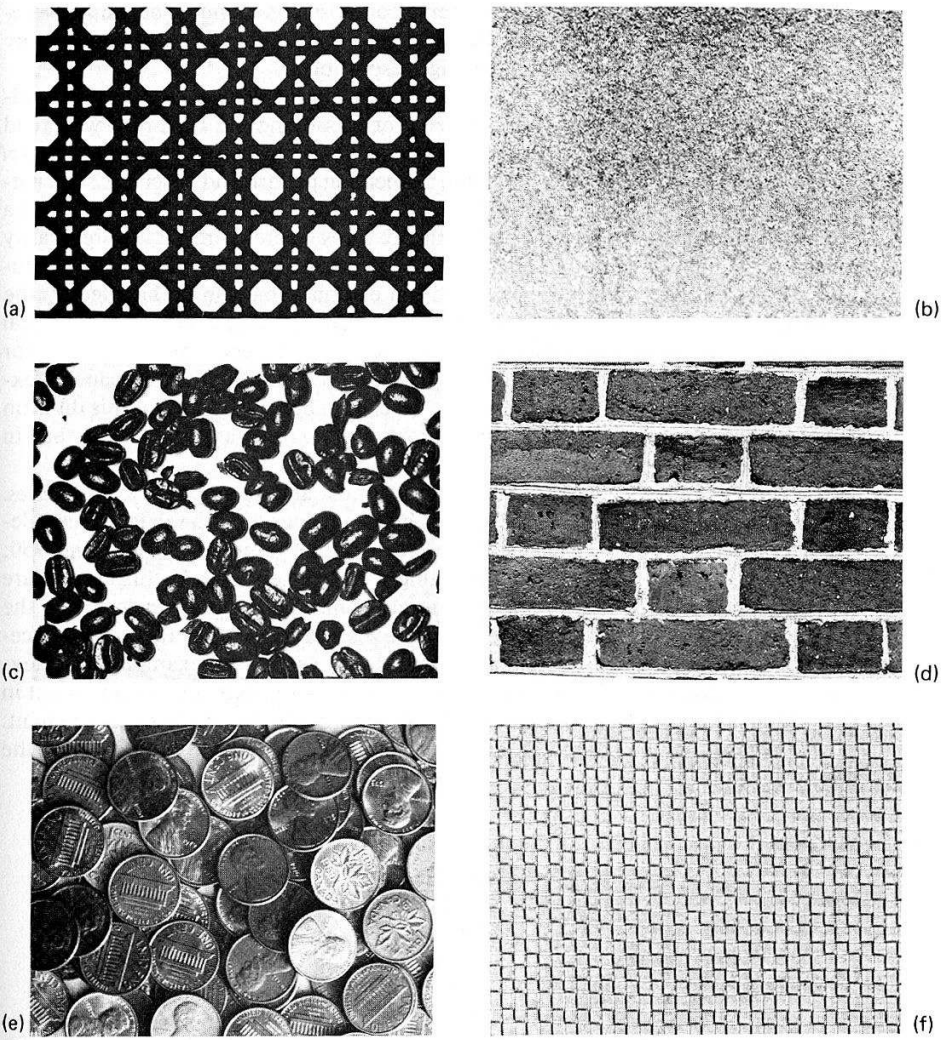

Fig. 6.1 Six examples of texture. (a) Cane. (b) Paper. (c) Coffee beans. (d) Brick wall. (e) Coins. (f) Wire braid.

The exposition of texture takes place under four main headings:

1. Texture primitives
2. Structural models
3. Statistical models
4. Texture gradients

We have already described texture as being composed of elements of *texture primitives.* The main point of additional discussion on texture primitives is to refine the idea of a primitive and its relation to image resolution.

The main work that is unique to texture is that which describes how primitives are related to the aim of recognizing or classifying the texture. Two broad classes of techniques have emerged and we shall study each in turn. The *structural* model regards the primitives as forming a repeating pattern and describes such patterns in terms of rules for generating them. Formally, these rules can be termed a grammar. This model is best for describing textures where there is much regularity in the placement of primitive elements and the texture is imaged at high resolution. The "reptile" texture in Fig. 6.9 is an example that can be handled by the structured approach. The *statistical* model usually describes texture by statistical rules governing the distribution and relation of gray levels. This works well for many natural textures which have barely discernible primitives. The "paper" texture is such an example. As we shall see, we cannot be too rigid about this division since statistical models can describe pattern-like textures and vice versa, but in general the dichotomy is helpful.

The examples suggest that texture is almost always a property of *surfaces.* Indeed, as the example of Fig. 6.2 shows, human beings tend to relate texture elements of varying size to a plausible surface in three dimensions [Gibson 1950; Stevens 1979]. Techniques for determining surface orientation in this fashion are termed texture *gradient* techniques. The gradient is given both in terms of the direction of greatest change in size of primitives and in terms of the spatial placement of primitives. The notion of a gradient is very useful. For example, if the texture is embedded on a flat surface, the gradient points toward a vanishing point in the image. The chapter concludes with algorithms for computing this gradient. The gradient may be computed directly or indirectly via the computation of the vanishing point.

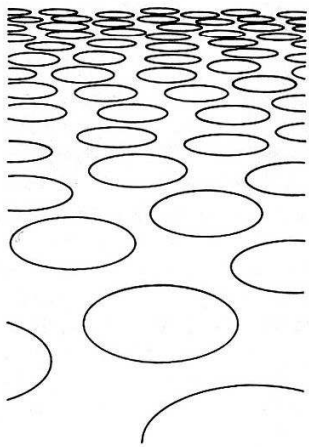

Fig. 6.2 Texture as a surface property.

6.2 TEXTURE PRIMITIVES

The notion of a primitive is central to texture. To highlight its importance, we shall use the appelation *texel* (for texture element) [Kender 1978]. A texel is (loosely) a visual primitive with certain invariant properties which occurs repeatedly in different positions, deformations, and orientations inside a given area. One basic invariant property of such a unit might be that its pixels have a constant gray level, but more elaborate properties related to shape are possible. (A detailed discussion of planar shapes is deferred until Chapter 8.) Figure 6.3 shows examples of two kinds of texels: (a) ellipses of approximately constant gray level and (b) linear edge segments. Interestingly, these are nearly the two features selected as texture primitives by [Julesz, 1981], who has performed extensive studies of human texture perception.

For textures that can be described in two dimensions, image-based descriptions are sufficient. Texture primitives may be pixels, or aggregates of pixels such as curve segments or regions. The "coffee beans" texture can be described by an image-based model: repeated dark ellipses on a lighter background. These models describe equally well an image of texture or an image of a picture of texture. The methods for creating these aggregates were discussed in Chapters 4 and 5. As with all image-based models, three-dimensional phenomena such as occlusion must be handled indirectly. In contrast, structural approaches to texture sometimes require knowledge of the three-dimensional world producing the texture image. One example of this is Brodatz's "coins" shown in Fig. 6.1. A three-dimensional model of the way coins can be stacked is needed to understand this texture fully.

An important part of the texel definition is that primitives must occur repeatedly inside a given area. The question is: How many times? This can be answered qualitatively by imagining a window that corresponds approximately to our field of view superimposed on a very large textured area. As this window is made smaller, corresponding to moving the viewpoint closer to the texture, fewer and fewer texels are contained in it. At some distance, the image in the window no longer

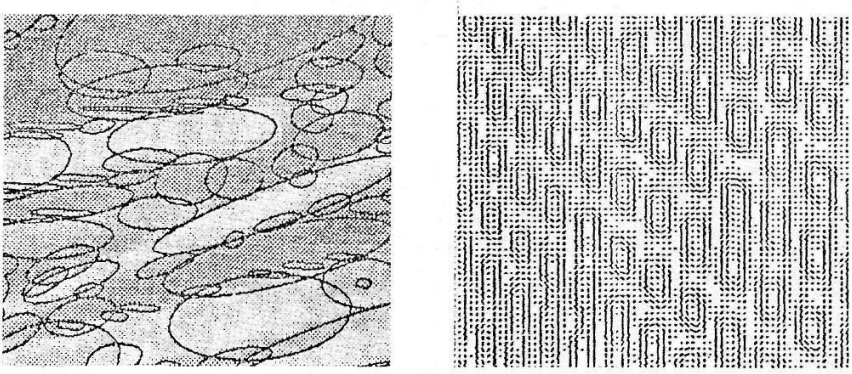

(a) (b)

Fig. 6.3 Examples of texels. (a) Ellipses. (b) Linear segments.

appears textured, or if it does, translation of the window changes the perceived texture drastically. At this point we no longer have a texture. A similar effect occurs if the window is made increasingly larger, corresponding to moving the field of view farther away from the image. At some distance textural details are blurred into continuous tones and repeated elements are no longer visible as the window is translated. (This is the basis for halftone images, which are highly textured patterns meant to be viewed from enough distance to blur the texture.) Thus the idea of an appropriate *resolution*, or the number of texels in a subimage, is an implicit part of our qualitative definition of texture. If the resolution is appropriate, the texture will be apparent and will "look the same" as the field of view is translated across the textured area. Most often the appropriate resolution is not known but must be computed. Often this computation is simpler to carry out than detailed computations characterizing the primitives and hence has been used as a precursor to the latter computations. Figure 6.4 shows such a resolution-like computation, which examines the image for repeating peaks [Connors 1979].

Textures can be hierarchical, the hierarchies corresponding to different resolutions. The "brick wall" texture shows such a hierarchy. At one resolution, the highly structured pattern made by collections of bricks is in evidence; at higher resolution, the variations of the texture of each brick are visible.

6.3 STRUCTURAL MODELS OF TEXEL PLACEMENT

Highly patterned textures tesselate the plane in an ordered way, and thus we must understand the different ways in which this can be done. In a regular tesselation the

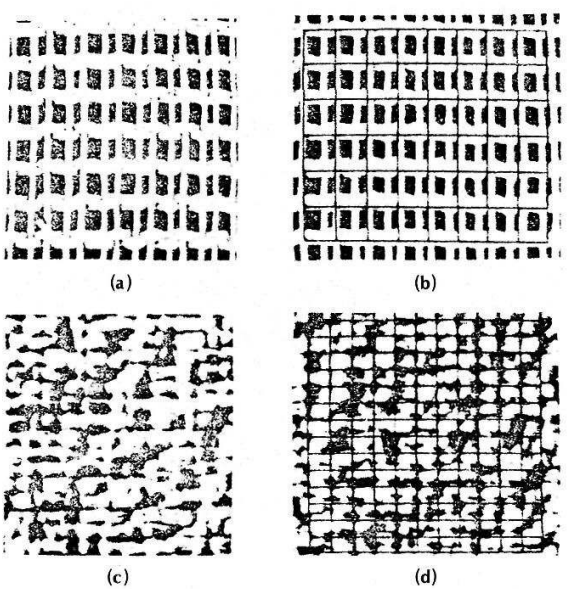

Fig. 6.4 Computing texture resolutions. (a) French canvas. (b) Resolution grid for canvas. (c) Raffia. (d) Grid for raffia.

polygons surrounding a vertex all have the same number of sides. Semiregular tesselations have two kinds of polygons (differing in number of sides) surrounding a vertex. Figure 2.11 depicts the regular tesselations of the plane. There are eight semiregular tesselations of the plane, as shown in Fig. 6.5. These tesselations are conveniently described by listing in order the number of sides of the polygons sur-

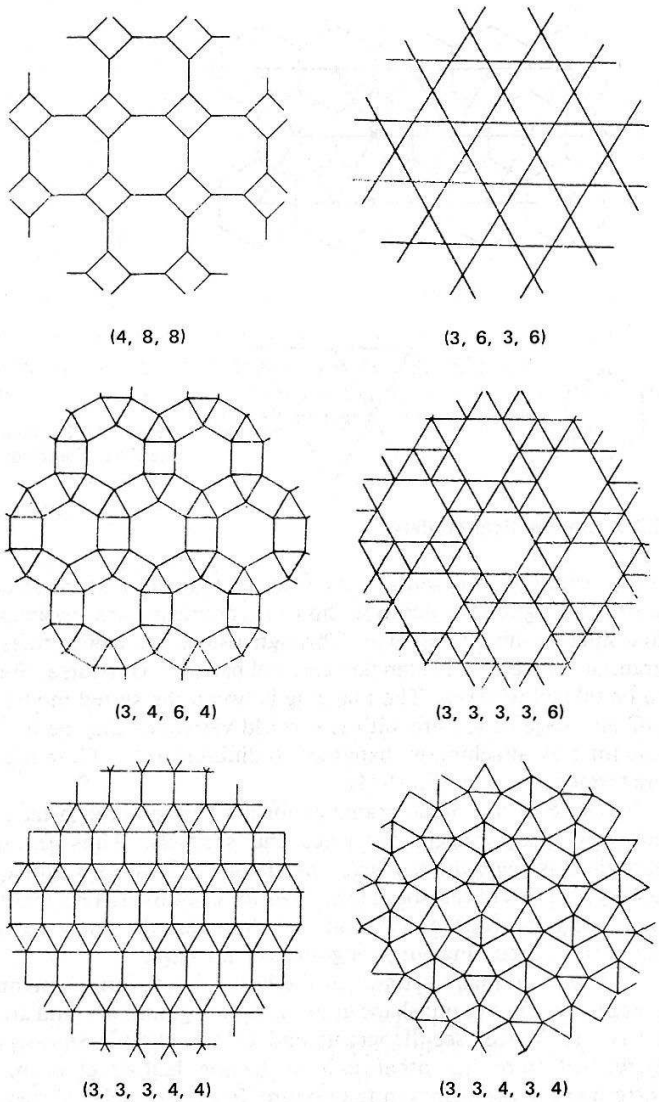

Fig. 6.5 Semiregular tesselations.

rounding each vertex. Thus a hexagonal tesselation is described by (6,6,6) and every vertex in the tesselation of Fig. 6.5 can be denoted by the list (3,12,12). It is important to note that the tesselations of interest are those which describe the *placement* of primitives rather than the primitives themselves. When the primitives define a tesselation, the tesselation describing the primitive placement will be the dual of this graph in the sense of Section 5.4. Figure 6.6 shows these relationships.

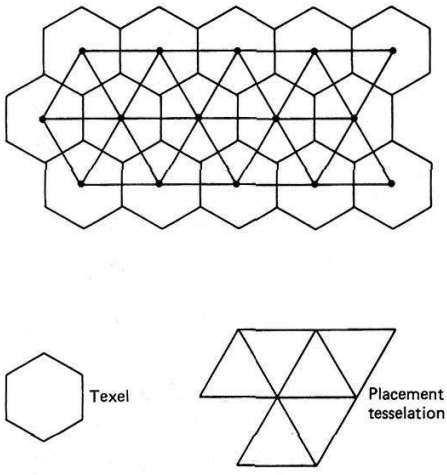

Fig. 6.6 The primitive placement tesselation as the dual of the primitive tesselation.

6.3.1 Grammatical Models

A powerful way of describing the rules that govern textural structure is through a grammar. A grammar describes how to generate patterns by applying *rewriting rules* to a small number of *symbols.* Through a small number of rules and symbols, the grammar can generate complex textural patterns. Of course, the symbols turn out to be related to texels. The mapping between the stored model prototype texture and an image of texture with real-world variations may be incorporated into the grammar by attaching probabilities to different rules. Grammars with such rules are termed *stochastic* [Fu 1974].

There is no unique grammar for a given texture; in fact, there are usually infinitely many choices for rules and symbols. Thus texture grammars are described as *syntactically ambiguous.* Figure 6.7 shows a syntactically ambiguous texture and two of the possible choices for primitives. This texture is also *semantically ambiguous* [Zucker 1976] in that alternate ridges may be thought of in three dimensions as coming out of or going into the page.

There are many variants of the basic idea of formal grammars and we shall examine three of them: shape grammars, tree grammars, and array grammars. For a basic reference, see [Hopcroft and Ullman 1979]. Shape grammars are distinguished from the other two by having high-level primitives that closely correspond to the shapes in the texture. In the examples of tree grammars and array grammars that we examine, texels are defined as pixels and this makes the

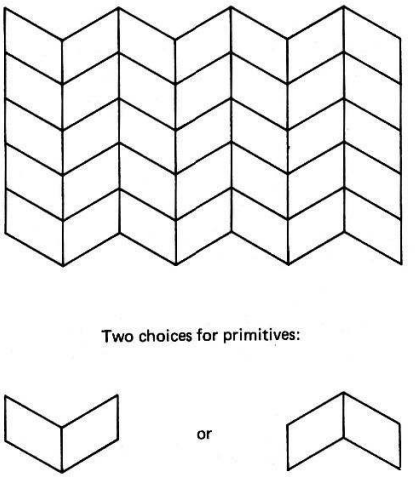

Fig. 6.7 Ambiguous texture.

grammars correspondingly more complicated. A particular texture that can be described in eight rules in a shape grammar requires 85 rules in a tree grammar [Lu and Fu 1978]. The compensating trade-off is that pixels are gratis with the image; considerable processing must be done to derive the more complex primitives used by the shape grammar.

6.3.2 Shape Grammars

A shape grammar [Stiny and Gips 1972] is defined as a four-tuple $< V_t, V_m, R, S>$ where:

1. V_t is a finite set of shapes
2. V_m is a finite set of shapes such that $V_t \cap V_m = \phi$
3. R is a finite set of ordered pairs (u, v) such that u is a shape consisting of elements of V_t^+ and v is a shape consisting of an element of V_t^* combined with an element of V_m^*
4. S is a shape consisting of an element of V_t^* combined with an element of V_m^*.

Elements of the set V_t are called terminal shape elements (or terminals). Elements of the set V_m are called nonterminal shape elements (or markers). The sets V_t and V_m must be disjoint. Elements of the set V_t^+ are formed by the finite arrangement of one or more elements of V_t in which any elements and/or their mirror images may be used a multiple number of times in any location, orientation, or scale. The set $V_t^* = V_t^+ \cup \{\Lambda\}$, where Λ is the empty shape. The sets V_m^+ and V_m^* are defined similarly. Elements (u, v) of R are called shape rules and are written $u\ v$. u is called the left side of the rule; v the right side of the rule. u and v usually are enclosed in identical dashed rectangles to show the correspondence between the two shapes. S is called the initial shape and normally contains a u such that there is a (u, v) which is an element of R.

A texture is generated from a shape grammar by beginning with the initial shape and repeatedly applying the shape rules. The result of applying a shape rule R to a given shape s is another shape, consisting of s with the right side of R substituted in S for an occurrence of the left side of R. Rule application to a shape proceeds as follows:

1. Find part of the shape that is geometrically similar to the left side of a rule in terms of both terminal elements and nonterminal elements (markers). There must be a one-to-one correspondence between the terminals and markers in the left side of the rule and the terminals and markers in the part of the shape to which the rule is to be applied.
2. Find the geometric transformations (scale, translation, rotation, mirror image) which make the left side of the rule identical to the corresponding part in the shape.
3. Apply those transformations to the right side of the rule.
4. Substitute the transformed right side of the rule for the part of the shape that corresponds to the left side of the rule.

The generation process is terminated when no rule in the grammar can be applied.

As a simple example, one of the many ways of specifying a hexagonal texture $\{V_t, V_m, R, S\}$ is

$V_t = \{$  $\}$

$V_m = \{ \cdot \}$ (6.1)

$R:$ 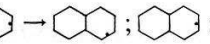 ;etc.

$S = \{$  $\}$

Hexagonal textures can be *generated* by the repeated application of the single rule in R. They can be *recognized* by the application of the rule in the opposite direction to a given texture until the initial shape, I, is produced. Of course, the rule will generate only hexagonal textures. Similarly, the hexagonal texture in Fig. 6.8a will be recognized but the variants in Fig. 6.8b will not.

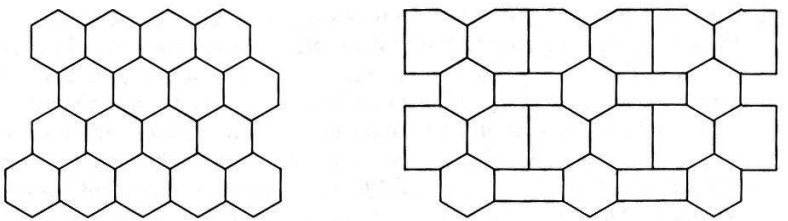

Fig. 6.8 Textures to be recognized (see text).

A more difficult example is given by the "reptile" texture. Except for the occasional new rows, a $(3, 6, 3, 6)$ tesselation of primitives would model this texture exactly. As shown in Fig. 6.9, the new row is introduced when a seven-sided polygon splits into a six-sided polygon and a five-sided polygon. To capture this with a shape grammar, we examine the dual of this graph, which is the primitive placement graph, Fig. 6.9b. This graph provides a simple explanation of how the extra row is created; that is, the diamond pattern splits into two. Notice that the dual graph is composed solely of four-sided polygons but that some vertices are $(4, 4, 4)$ and some are $(4, 4, 4, 4, 4, 4)$. A shape grammar for the dual is shown in Fig. 6.10. The image texture can be obtained by forming the dual of this graph. One further refinement should be added to rules (6) and (7); so that rule (7) is used less often, the appropriate probabilities should be associated with each rule. This would make the grammar stochastic.

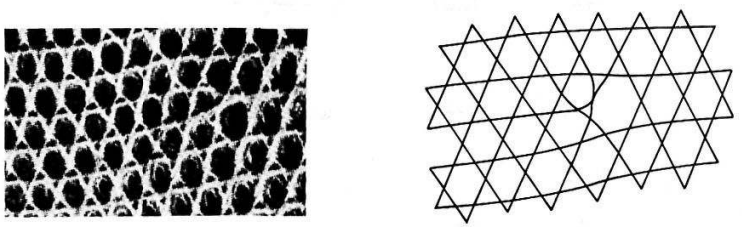

Fig. 6.9 (a) The reptile texture. (b) The reptile texture as a $(3, 6, 3, 6)$ semiregular tesselation with local deformations.

6.3.3 Tree Grammars

The symbolic form of a tree grammar is very similar to that of a shape grammar. A grammar

$$G_t = (V_t, V_m, r, R, S)$$

is a tree grammar if

V_t is a set of terminal symbols
V_m is a set of symbols such that
$V_m \cap V_t = \phi$
$r : V_t \rightarrow N$ (where N is the set of nonnegative integers)
is the rank associated with symbols in V_t
S is the start symbol
R is the set of rules of the form

$$X_0 \rightarrow x \qquad \text{or} \qquad X_0 \rightarrow x$$
$$\quad\;\; | \;\diagdown$$
$$X_0 \ldots X_{r(x)}$$

with x in V_t and $X_0 \ldots X_{r(x)}$ in V_m

For a tree grammar to generate arrays of pixels, it is necessary to choose some way of embedding the tree in the array. Figure 6.11 shows two such embeddings.

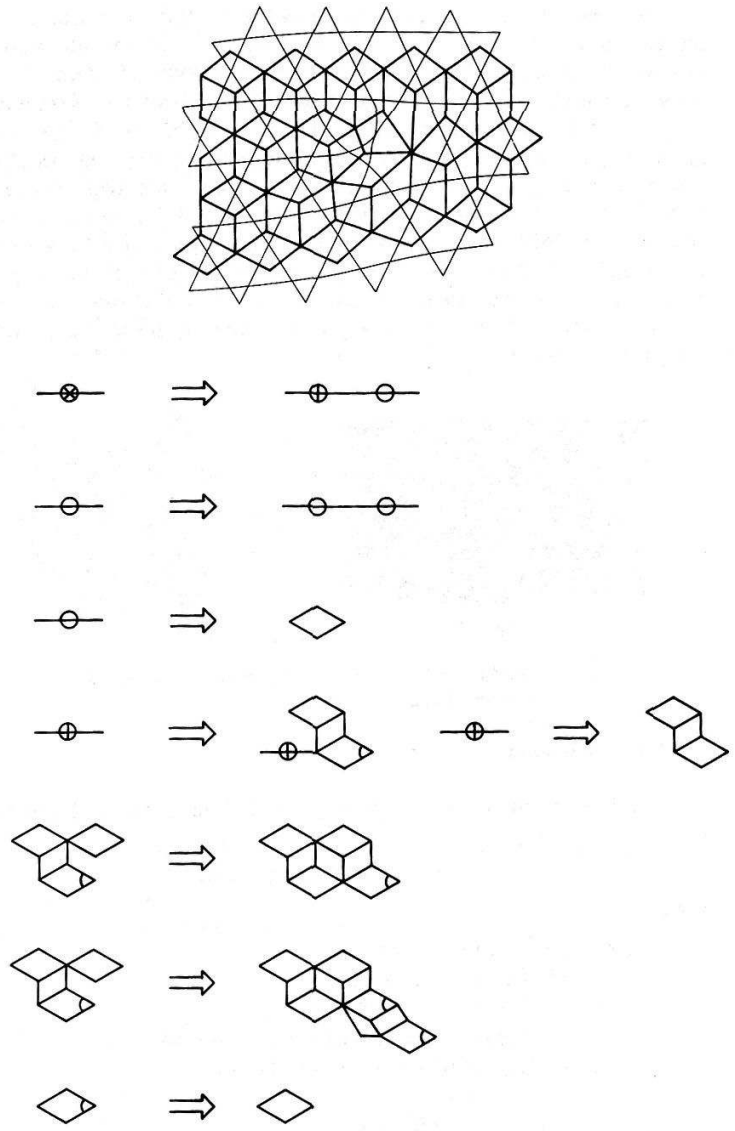

Fig. 6.10 Shape grammar for the reptile texture.

In the application to texture [Lu and Fu 1978], the notion of pyramids or hierarchical levels of resolution in texture is used. One level describes the placement of repeating patterns in texture windows—a rectangular texel placement tesselation—and another level describes texels in terms of pixels. We shall illus-

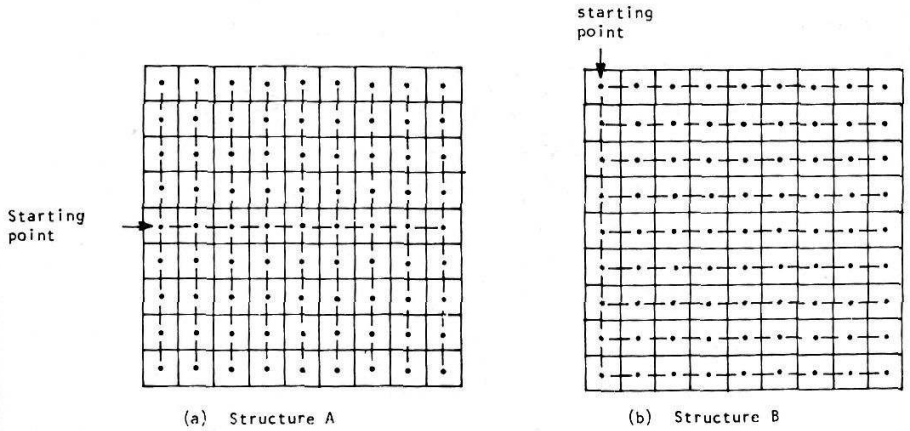

Fig. 6.11 *Two ways of embedding a tree structure in an array.*

trate these ideas with Lu and Fu's grammar for "wire braid." The texture windows are shown in Fig. 6.12a. Each of these can be described by a "sentence" in a second tree grammar. The grammar is given by:

$$G_w = (V_t, V_m, r, R, S)$$

where

$$\begin{aligned} V_t &= \{A_1, C_1\} \\ V_m &= \{X, Y, Z\} \\ r &= \{0, 1, 2\} \\ R: X &\rightarrow \overset{X \quad Y}{A_1} \quad \text{or} \quad \overset{Y}{A_1} \\ Y &\rightarrow \overset{Z}{C_1} \quad \text{or} \quad C_1 \\ Z &\rightarrow \overset{Y}{A_1} \quad \text{or} \quad A_1 \end{aligned} \tag{6.2}$$

and the first embedding in Fig. 6.11 is used. The pattern inside each of these windows is specified by another grammatical level:

$$G = (V_t, V_m, r, R, S)$$

where

$$V_t = \{1, 0\}$$

$$V_m = \{A_1, A_2, A_3, A_4, A_5, A_6, A_7, C_1, C_2, C_3, C_4, C_5, C_6, C_7, N_0, N_1, N_2, N_3, N_4\}$$

$$r = \{0, 1, 2\}$$

$$S = \{A_1, C_1\}$$

R:

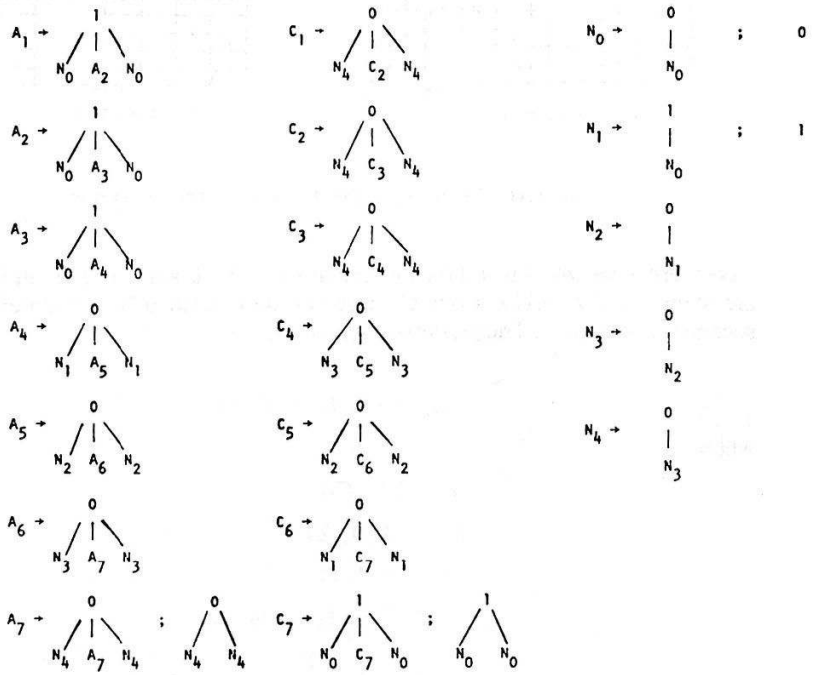

The application of these rules generates the two different patterns of pixels shown in Fig. 6.13.

6.3.4 Array Grammars

Like tree grammars, array grammars use hierarchical levels of resolution [Milgram and Rosenfeld 1971; Rosenfeld 1971]. Array grammars are different from tree grammars in that they do not use the tree-array embedding. Instead, prodigious use of a blank or null symbol is used to make sure the rules are applied in appropriate contexts. A simple array grammar for generating a checkerboard pattern is

$$G = \{V_t, V_n, R\}$$

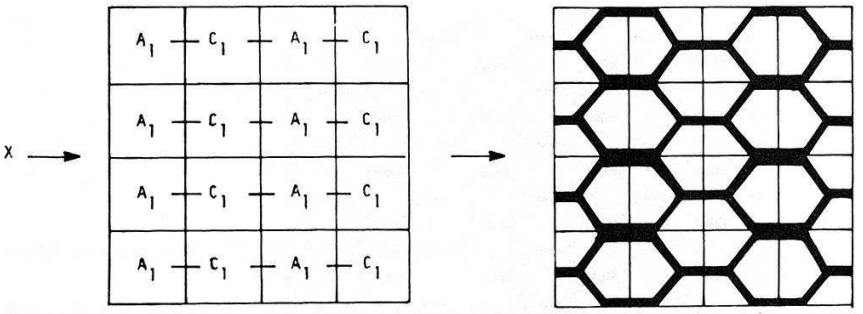

Fig. 6.12 Texture window and grammar (see text).

where

$$V_t = \{0, 1\} \text{ (corresponding to black and white pixels, respectively)}$$
$$V_n = \{b, S\}$$

b is a "blank" symbol used to provide context for the application of the rules. Another notational convenience is to use a subscript to denote the orientation of symbols. For example, when describing the rules R we use

$$0_x b \rightarrow 0_x 1 \qquad \text{where } x \text{ is one of } \{U, D, L, R\}$$

to summarize the four rules

$$\begin{matrix} 0 \\ b \end{matrix} \rightarrow \begin{matrix} 0 \\ 1 \end{matrix}, \qquad \begin{matrix} b \\ 0 \end{matrix} \rightarrow \begin{matrix} 1 \\ 0 \end{matrix}, \qquad 0b \rightarrow 01, \qquad b0 \rightarrow 10$$

Thus the checkerboard rule set is given by

$$R: S \rightarrow 0 \text{ or } 1$$
$$0_x b \rightarrow 0_x 1 \qquad x \text{ in } \{U, D, L, R\}$$
$$1_x b \rightarrow 1_x 0$$

A compact encoding of textural patterns [Jayaramamurthy 1979] uses levels of array grammars defined on a pyramid. The terminal symbols of one layer are the start symbols of the next grammatical layer defined lower down in the pyramid. This corresponds nicely to the idea of having one grammar to generate primitives and another to generate the primitive placement tesselations.

As another example, consider the herringbone pattern in Fig. 6.14a, which is composed of 4×3 arrays of a particular placement pattern as shown in Fig. 6.14b. The following grammar is sufficient to generate the placement pattern.

$$G_w = \{V_t, V_m, R, S\}$$

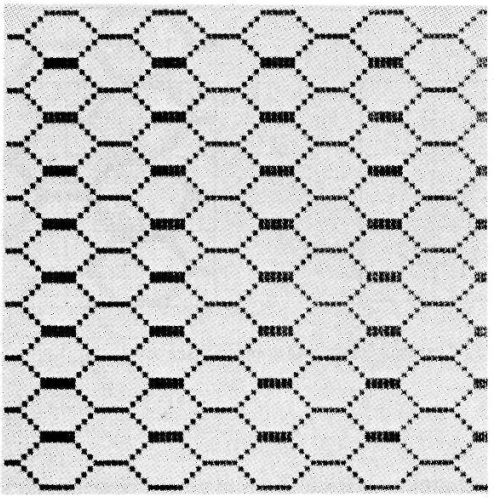

Fig. 6.13 Texture generated by tree grammar.

where

$$V_t = \{a\}$$

$$V_n = \{b, S\}$$

$$R: S \rightarrow a$$

$$a_x b \rightarrow a_x a \qquad x \text{ in } \{U, D, L, R\}$$

We have not been precise in specifying how the terminal symbol is projected onto the lower level. Assume without loss of generality that it is placed in the upper left-hand corner, the rest of the subarray being initially blank symbols. Thus a simple grammar for the primitive is

$$G_t = \{V_t, V_n, R, S\}$$

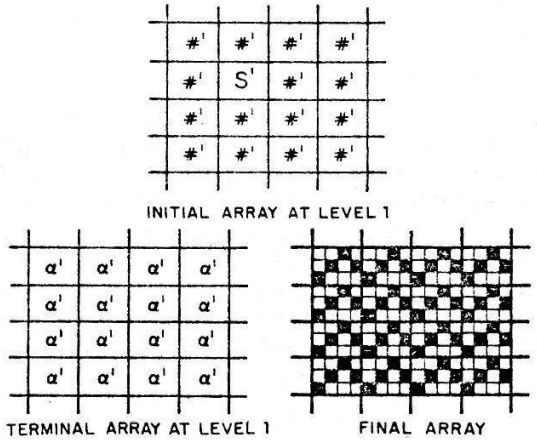

Fig. 6.14 Steps in generating a herringbone texture with an array grammar.

where

$$V_t = \{0, 1\}$$

$$V_n = \{a, b\}$$

$$R: \begin{matrix} a & b & b & b \\ b & b & b & b \\ b & b & b & b \end{matrix} \rightarrow \begin{matrix} 0 & 0 & 1 & 0 \\ 0 & 1 & 0 & 1 \\ 1 & 0 & 0 & 0 \end{matrix}$$

6.4 TEXTURE AS A PATTERN RECOGNITION PROBLEM

Many textures do not have the nice geometrical regularity of "reptile" or "wire braid"; instead, they exhibit variations that are not satisfactorily described by shapes, but are best described by statistical models. *Statistical pattern recognition* is a paradigm that can classify statistical variations in patterns. (There are other statistical methods of describing texture [Pratt et al. 1981], but we will focus on statistical pattern recognition since it is the most widely used for computer vision purposes.) There is a voluminous literature on pattern recognition, including several excellent texts (e.g., [Fu 1968; Tou and Gonzalez 1974; Fukunaga 1972], and the ideas have much wider application than their use here, but they seem particularly appropriate for low-resolution textures, such as those seen in aerial images [Weszka et al. 1976]. The pattern recognition approach to the problem is to classify instances of a texture in an image into a set of classes. For example, given the textures in Fig. 6.15, the choice might be between the classes "orchard," "field," "residential," "water."

The basic notion of pattern recognition is the *feature vector.* The feature vector $\mathbf{v}$ is a set of measurements $\{v_1 \cdots v_m\}$ which is supposed to condense the description of relevant properties of the textured image into a small, Euclidean *feature space* of m dimensions. Each point in feature space represents a value for the feature vector applied to a different image (or subimage) of texture. The measurement values for a feature should be correlated with its class membership. Figure 6.16 shows a two-dimensional space in which the features exhibit the desired correlation property. Feature vector values cluster according to the texture from which they were derived. Figure 6.16 shows a bad choice of features (measurements) which does not separate the different classes.

The pattern recognition paradigm divides the problem into two phases: training and test. Usually, during a training phase, feature vectors from known samples are used to partition feature space into regions representing the different classes. However, self teaching can be done; the classifier derives its own partitions. Feature selection can be based on parametric or nonparametric models of the distributions of points in feature space. In the former case, analytic solutions are sometimes available. In the latter, feature vectors are *clustered* into groups which are taken to indicate partitions. During a test phase the feature-space partitions are used to classify feature vectors from unknown samples. Figure 6.17 shows this process.

Given that the data are reasonably well behaved, there are many methods for clustering feature vectors [Fukunaga 1972; Tou and Gonzales 1974; Fu 1974].

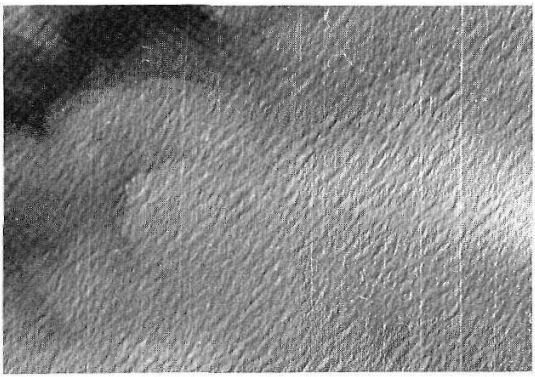

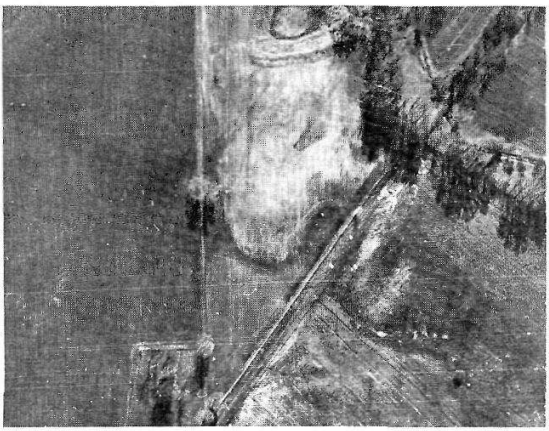

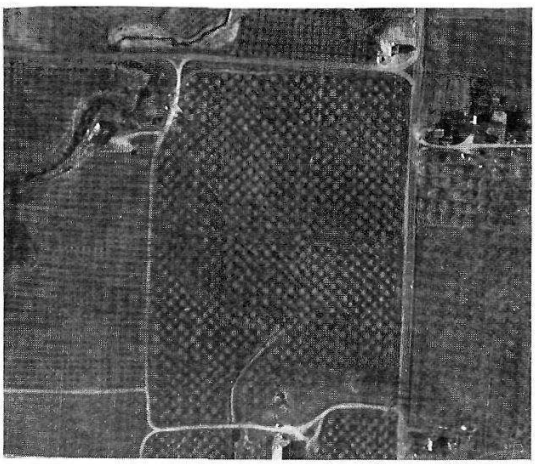

Fig. 6.15 Aerial image textures for discrimination.

Fig. 6.15 (cont.)

One popular way of doing this is to use prototype points for each class and a *nearest-neighbor* rule [Cover 1968]:

assign $\mathbf{v}$ to class w_i if i minimizes
$\min_i d(\mathbf{v}, \mathbf{v}_{w_i})$

where $\mathbf{v}_{w_i}$ is the prototype point for class w_i.

Parametric techniques assume information about the feature vector probability distributions to find rules that maximize the likelihood of correct classification:

assign $\mathbf{v}$ to class w_i if i maximizes
$\max_i p(w_i|\mathbf{v})$

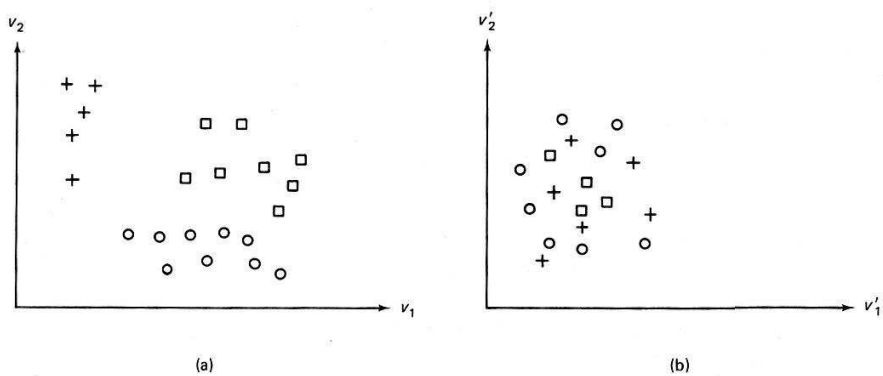

Fig. 6.16 Feature space for texture discrimination. (a) effective features (b) ineffective features.

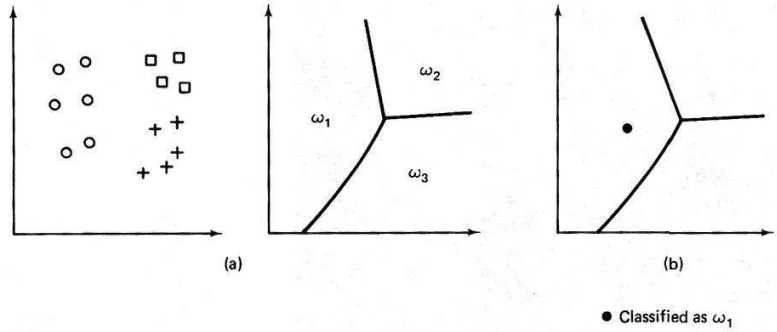

Fig. 6.17 Pattern recognition paradigm.

The distributions may also be used to formulate rules that minimize errors.

Picking good features is the essence of pattern recognition. No elaborate formalism will work well for bad features such as those of Fig. 6.15b. On the other hand, almost any method will work for very good features. For this reason, texture is a good domain for pattern recognition: it is fairly easy to define features that (1) cluster in feature space according to different classes, and (2) can separate texture classes.

The ensuing subsections describe features that have worked well. These subsections are in reverse order from those of Section 6.2 in that we begin with features defined on pixels—Fourier subspaces, gray-level dependencies—and conclude with features defined on higher-level texels such as regions. However, the lesson is the same as with the grammatical approach: hard work spent in obtaining high-level primitives can both improve and simplify the texture model. Space does not permit a discussion of many texture features; instead, we limit ourselves to a few representative samples. For further reading, see [Haralick 1978].

6.4.1 Texture Energy

Fourier Domain Basis

If a texture is at all spatially periodic or directional, its power spectrum will tend to have peaks for corresponding spatial frequencies. These peaks can form the basis of features of a pattern recognition discriminator. One way to define features is to search Fourier space directly [Bajcsy and Lieberman 1976]. Another is to partition Fourier space into bins. Two kinds of bins, radial and angular, are commonly used, as shown in Fig. 6.18. These bins, together with the Fourier power spectrum are used to define features. If F is the Fourier transform, the Fourier power spectrum is given by $|F|^2$.

Radial features are given by

$$v_{r_1 r_2} = \int\int |F(u, v)|^2 \, du \, dv \tag{6.5}$$

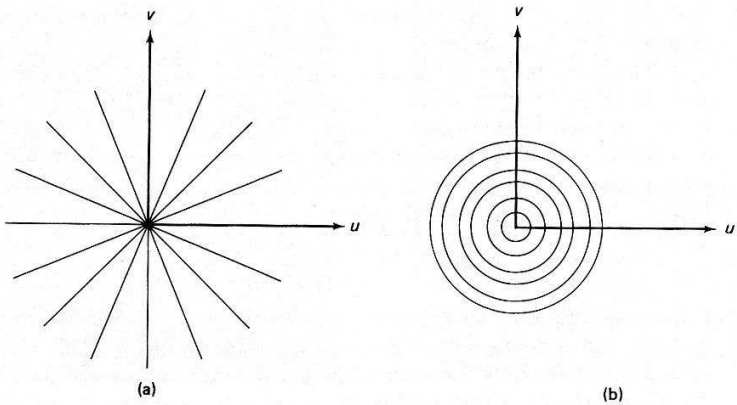

Fig. 6.18 Partitioning the Fourier domain into bins.

where the limits of integration are defined by

$$r_1^2 \leqslant u^2 + v^2 < r_2^2$$
$$0 \leqslant u, v < n-1$$

where $[r_1, r_2]$ is one of the radial bins and $\mathbf{v}$ is the vector (not related to v) defined by different values of r_1 and r_2. Radial features are correlated with texture coarseness. A smooth texture will have high values of $V_{r_1 r_2}$ for small radii, whereas a coarse, grainy texture will tend to have relatively higher values for larger radii.

Features that measure angular orientation are given by

$$\mathbf{v}_{\theta_1 \theta_2} = \int\int |F(u, v)|^2 \, du \, dv \tag{6.6}$$

where the limits of integration are defined by

$$\theta_1 \leqslant \tan^{-1}\left(\frac{v}{u}\right) < \theta_2$$
$$0 < u, v \leqslant n-1$$

where $[\theta_1, \theta_2)$ is one of the sectors and $\mathbf{v}$ is defined by different values of θ_1 and θ_2. These features exploit the sensitivity of the power spectrum to the directionality of the texture. If a texture has as many lines or edges in a given direction θ, $|F|^2$ will tend to have high values clustered around the direction in frequency space $\theta + \pi/2$.

Texture Energy in the Spatial Domain

From Section 2.2.4 we know that the Fourier approach could also be carried out in the image domain. This is the approach taken in [Laws 1980]. The advantage of this approach is that the basis is not the Fourier basis but a variant that is more

matched to intuition about texture features. Figure 6.19 shows the most important of Laws' 12 basis functions.

The image is first histogram-equalized (Section 3.2). Then 12 new images are made by convolving the original image with each of the basis functions (i.e., $f_k' = f * h_k$ for basis functions $h_1, \ldots, h_{12}$). Then each of these images is transformed into an "energy" image by the following transformation: Each pixel in the convolved image is replaced by an average of the absolute values in a local window of 15×15 pixels centered over the pixel:

$$f_k''(x, y) = \sum_{x', y' \text{ in window}} (|f_k'(x', y')|) \tag{6.7}$$

The transformation $f \rightarrow f_k''$, $k = 1, \ldots 12$ is termed a "texture energy transform" by Laws and is analogous to the Fourier power spectrum. The f_k'', $k = 1, \ldots 12$ form a set of features for each point in the image which are used in a nearest-neighbor classifier. Classification details may be found in [Laws 1980]. Our interest is in the particular choice of basis functions used.

Figure 6.20 shows a composite of natural textures [Brodatz 1966] used in Laws's experiments. Each texture is digitized into a 128×128 pixel subimage. The texture energy transforms were applied to this composite image and each pixel was classified into one of the eight categories. The average classification accuracy was about 87% for interior regions of the subimages. This is a very good result for textures that are similar.

6.4.2 Spatial Gray-Level Dependence

Spatial gray-level dependence (SGLD) matrices are one of the most popular sources of features [Kruger et al. 1974; Hall et al. 1971; Haralick et al. 1973]. The SGLD approach computes an intermediate matrix of measures from the digitized image data, and then defines features as functions on this intermediate matrix. Given an image f with a set of discrete gray levels I, we define for each of a set of discrete values of d and θ the intermediate matrix $S(d, \theta)$ as follows:

> $S(i, j|d, \theta)$, an entry in the matrix, is the number of times gray level i is oriented with respect to gray level j such that where
>
> $$f(\mathbf{x}) = i \quad \text{and} \quad f(\mathbf{y}) = j \quad \text{then}$$
>
> $$\mathbf{y} = \mathbf{x} + (d\cos\theta,\ d\sin\theta)$$

$$\begin{bmatrix} -1 & -4 & -6 & -4 & -1 \\ -2 & -8 & -12 & -8 & -2 \\ 0 & 0 & 0 & 0 & 0 \\ 2 & 8 & 12 & 8 & 2 \\ 1 & 4 & 6 & 4 & 1 \end{bmatrix} \qquad \begin{bmatrix} 1 & -4 & 6 & -4 & 1 \\ -4 & 16 & -24 & 16 & -4 \\ 6 & -24 & 36 & -24 & 6 \\ -4 & 16 & -24 & 16 & -4 \\ 1 & -4 & 6 & -4 & 1 \end{bmatrix}$$

$$\begin{bmatrix} -1 & 0 & 2 & 0 & -1 \\ -2 & 0 & 4 & 0 & -2 \\ 0 & 0 & 0 & 0 & 0 \\ 2 & 0 & -4 & 0 & 2 \\ 1 & 0 & -2 & 0 & 1 \end{bmatrix} \qquad \begin{bmatrix} -1 & 0 & 2 & 0 & -1 \\ -4 & 0 & 8 & 0 & -4 \\ -6 & 0 & 12 & 0 & -6 \\ -4 & 0 & 8 & 0 & -4 \\ -1 & 0 & 2 & 0 & -1 \end{bmatrix}$$

Fig. 6.19 Laws' basis functions (these are the low-order four of twelve actually used).

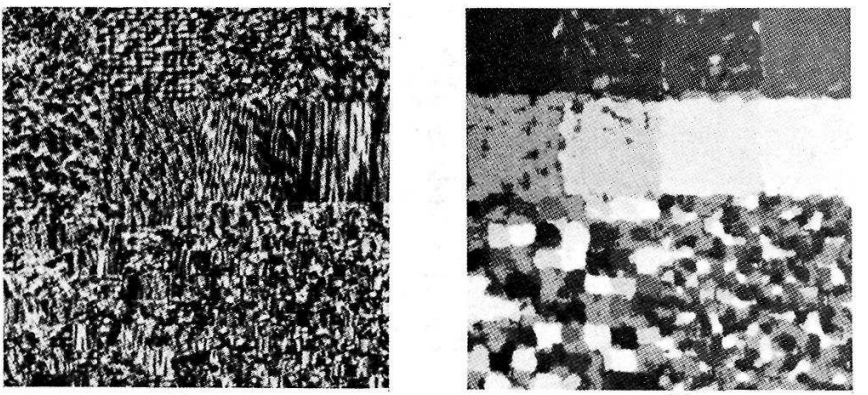

(a) (b)

Fig. 6.20 (a) Texture composite. (b) Classification.

Note that we the gray-level values appear as indices of the matrix S, implying that they are taken from some well-ordered discrete set 0, ..., K. Since

$$S(d, \theta) = S(d, \theta + \pi).$$

common practice is to restrict θ to multiples of $\pi/4$. Furthermore, information is not usually retained at both θ and $\theta + \pi$. The reasoning for the latter step is that for most texture discrimination tasks, the information is redundant. Thus we define

$$S(d, \theta) = \tfrac{1}{2} [S(d, \theta) + S(d, \theta + \pi)]$$

The intermediate matrices S yield potential features. Commonly used features are:

1. *Energy*

$$E(d, \theta) = \sum_{i=0}^{K} \sum_{j=0}^{K} [S(i, j|d, \theta)]^2 \tag{6.8}$$

2. *Entropy*

$$H(d, \theta) = \sum_{i=0}^{K} \sum_{j=0}^{K} S(i, j|d, \theta) \log f(i, j|d, \theta) \tag{6.9}$$

3. *Correlation*

$$C(d, \theta) = \frac{\sum_{i=0}^{K} \sum_{j=0}^{K} (i-\mu_x)(j-\mu_y) S(i, j|d, \theta)}{\sigma_x \sigma_y} \tag{6.10}$$

4. *Inertia*

$$I(d, \theta) = \sum_{i=0}^{K} \sum_{j=0}^{K} (i-j)^2 S(i, j|d, \theta) \tag{6.11}$$

5. *Local Homogeneity*

$$L(d, \theta) = \sum_{i=0}^{K} \sum_{j=0}^{K} \frac{1}{1 + (i-j)^2} S(i, j|d, \theta) \tag{6.12}$$

where $S(i, j|d, \theta)$ is the (i, j) th element of (d, θ), and

$$\mu_x = \sum_{i=0}^{K} i \sum_{j=0}^{K} S(i, j|d, \theta) \tag{6.13a}$$

$$\mu_y = \sum_{i=0}^{K} j \sum_{j=0}^{K} S(i, j|d, \theta) \tag{6.13b}$$

$$\sigma_x^2 = \sum_{i=0}^{K} (i-\mu_x)^2 \sum_{j=0}^{K} f(i, j|d, \theta) \tag{6.13c}$$

and

$$\sigma_y^2 = \sum_{i=0}^{K} (j-\mu_y)^2 \sum_{i=0}^{K} f(i, j|d, \theta) \tag{6.13d}$$

One important aspect of this approach is that the features chosen do not have psychological correlates [Tamura et al. 1978]. For example, none of the measures described would take on specific values corresponding to our notions of "rough" or "smooth." Also, the texture gradient is difficult to define in terms of SGLD feature values [Bajcsy and Lieberman 1976].

6.4.3 Region Texels

Region texels are an image-based way of defining primitives above the level of pixels. Rather than defining features directly as functions of pixels, a region segmentation of the image is created first. Features can then be defined in terms of the shape of the resultant regions, which are often more intuitive than the pixel-related features. Naturally, the approach of using edge elements is also possible. We shall discuss this in the context of texture gradients.

The idea of using regions as texture primitives was pursued in [Maleson et al. 1977]. In that implementation, all regions are ultimately modeled as ellipses and a corresponding five-parameter shape description is computed for each region. These parameters only define gross region shape, but the five-parameter primitives seem to work well for many domains. The texture image is segmented into regions in two steps. Initially, the modified version of Algorithm 5.1 that works for gray-level images is used. Figure 6.21 shows this example of the segmentation applied to a sample of "straw" texture. Next, parameters of the region grower are controlled so as to encourage convex regions which are fit with ellipses. Figure 6.22 shows the resultant ellipses for the "straw" texture. One set of ellipse parameters is $\mathbf{x}_0, a, b, \theta$ where $\mathbf{x}_0$ is the origin, a and b are the major and minor axis lengths and θ is the orientation of the major axis (Appendix 1). Besides these shape parameters, elliptical texels are also described by their average gray level. Figure 6.23 gives a qualitative indication of how ranges on feature values reflect different texels.

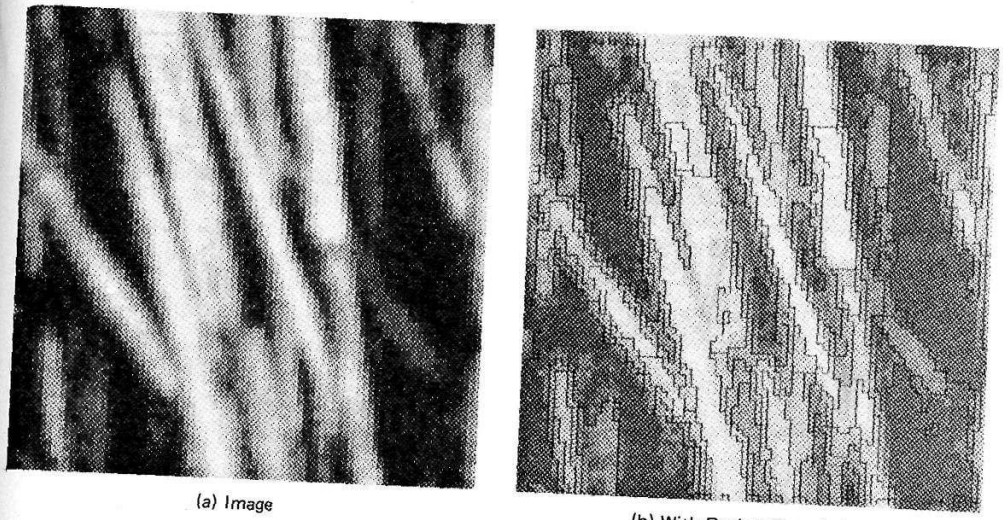

(a) Image (b) With Region Boundaries

Fig. 6.21 Region segmentation for straw texture.

6.5 THE TEXTURE GRADIENT

The importance of texture in determining surface orientation was described by Gibson [Gibson 1950]. There are three ways in which this can be done. These methods are depicted in Fig. 6.24. All these methods assume that the texture is embedded on a planar surface.

First, if the texture image has been segmented into primitives, the maximum rate of change of the projected size of these primitives constrains the orientation of

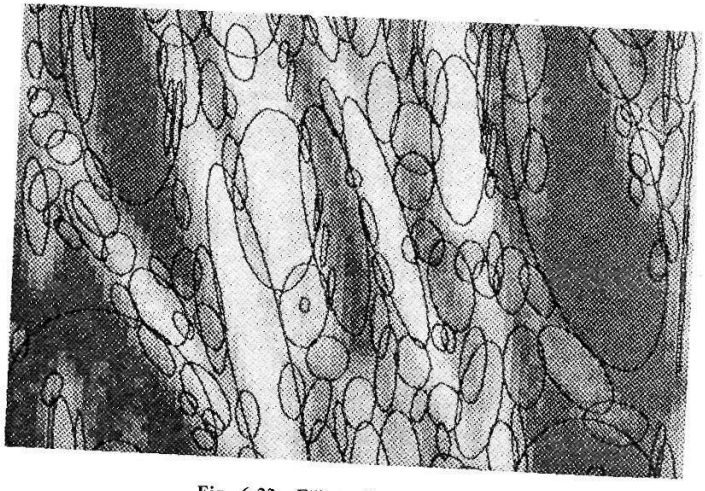

Fig. 6.22 Ellipses for straw texture.

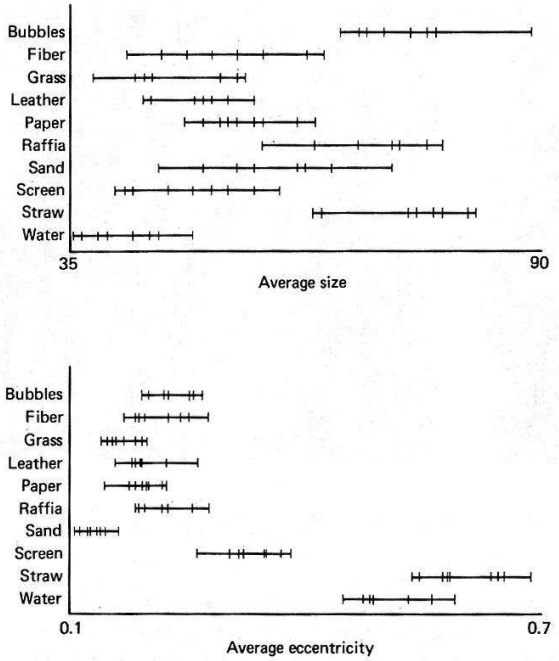

Fig. 6.23 Features defined on ellipses.

the plane in the following manner. The direction of maximum rate of change of projected primitive size is the direction of the *texture gradient.* The orientation of this direction with respect to the image coordinate frame determines how much the plane is rotated about the camera line of sight. The magnitude of the gradient can help determine how much the plane is tilted with respect to the camera, but knowledge about the camera geometry is also required. We have seen these ideas before in the form of gradient space; the rotation and tilt characterization is a polar coordinate representation of gradients.

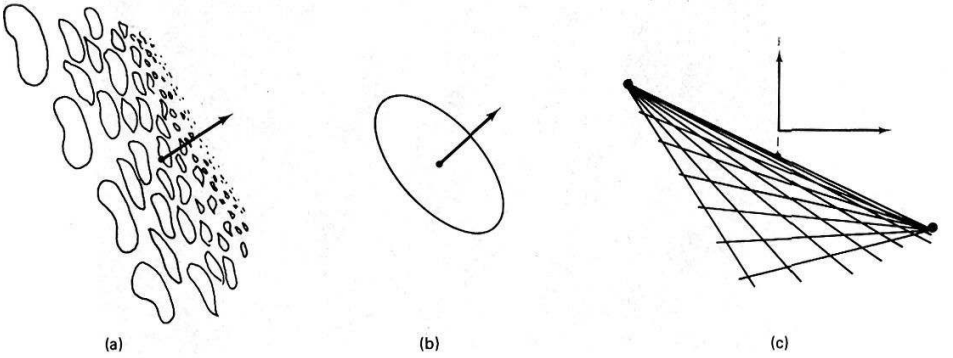

Fig. 6.24 Methods for calculating surface orientation from texture.

The second way to measure surface orientation is by knowing the shape of the texel itself. For example, a texture composed of circles appears as ellipses on the tilted surface. The orientation of the principal axes defines rotation with respect to the camera, and the ratio of minor to major axes defines tilt [Stevens 1979].

Finally, if the texture is composed of a regular grid of texels, we can compute vanishing points. For a perspective image, vanishing points on a plane P are the projection onto the image plane of the points at infinity in a given direction. In the examples here, the texels themselves are (conveniently) small line segments on a plane that are oriented in two orthogonal directions in the physical world. The general method applies whenever the placement tesselation defines lines of texels. Two vanishing points that arise from texels on the same surface can be used to determine orientation as follows. The line joining the vanishing points provides the orientation of the surface and the vertical position of the plane with respect to the z axis (i.e., the intersection of the line joining the vanishing points with $x = 0$) determines the tilt of the plane.

Line segment textures indicate vanishing points [Kender 1978]. As shown in Fig. 6.25, these segments could arise quite naturally from an urban image of the windows of a building which has been processed with an edge operator.

As discussed in Chapter 4, lines in images can be detected by detecting their parameters with a Hough algorithm. For example, by using the line parameterization

$$x \cos\theta + y \sin\theta = r$$

and by knowing the orientation of the line in terms of its gradient $\mathbf{g} = (\Delta x, \Delta y)$, a line segment $(x, y, \Delta x, \Delta y)$ can be mapped into r, θ space by using the relations

$$r = \frac{\Delta x x + \Delta y y}{\sqrt{\Delta x^2 + \Delta y^2}} \tag{6.14}$$

$$\theta = \tan^{-1}\left(\frac{\Delta y}{\Delta x}\right) \tag{6.15}$$

These relationships can be derived by using Fig. 6.26 and some geometry. The Cartesian coordinates of the $r-\theta$ space vector are given by

$$\mathbf{a} = \left(\frac{\mathbf{g}\cdot\mathbf{x}}{\|\mathbf{g}\|^2}\right)\mathbf{g} \tag{6.16}$$

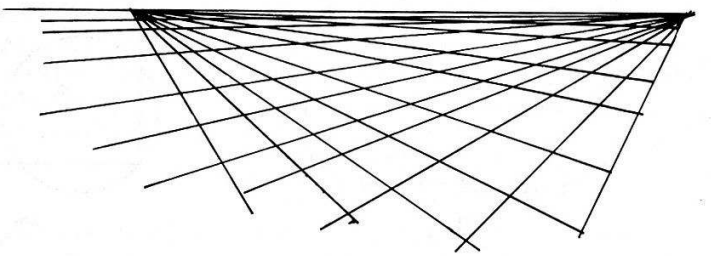

Fig. 6.25 Orthogonal line segments comprising a texture.

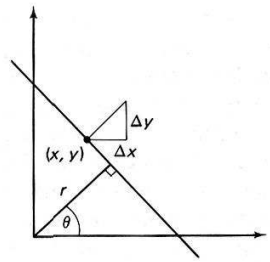

Fig. 6.26 r-θ transform.

Using this transformation, the set of line segments L_1 shown in Fig. 6.27 are all mapped into a single point in $r-\theta$ space. Furthermore, the set of lines L_2 which have the same vanishing point (x_v, y_v) project onto a circle in $r-\theta$ space with the line segment $((0, 0), (x_v, y_v))$ as a diameter. This scheme has two drawbacks: (1) vanishing points at infinity are projected into infinity, and (2) circles require some effort to detect. Hence we are motivated to use the transform $(x, y, \Delta x, \Delta y) \rightarrow \left(\frac{k}{r}, \theta\right)$ for some constant k. Now vanishing points at infinity are projected into the origin and the locus of the set of points L_2 is now a line. This line is perpendicular to the vector $\boldsymbol{x}_v$ and $\frac{k}{\|\mathbf{x}_v\|}$ units from the origin, as shown in Fig. 6.28. It can be detected by a second stage of the Hough transform; each point **a** is mapped into an $r'-\theta'$ space. For every **a**, compute all the r', θ' such that

$$a \cos\theta' + b \sin\theta' = r' \tag{6.17}$$

and increment that location in the appropriate r', θ' accumulator array. In this second space a vanishing point is detected as

$$r' = \frac{k}{\|\mathbf{x}_v\|} \tag{6.18}$$

$$\theta' = \tan^{-1}\left(\frac{y_v}{x_v}\right) \tag{6.19}$$

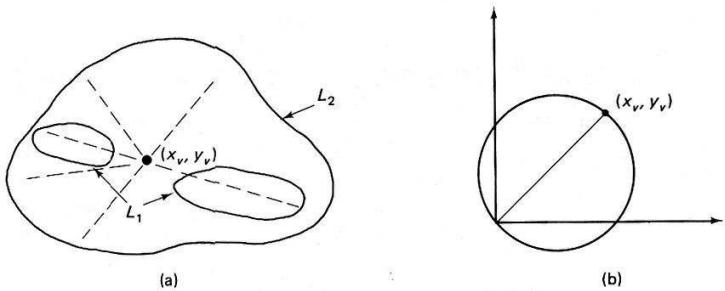

Fig. 6.27 Detecting the vanishing point with the Hough transform.

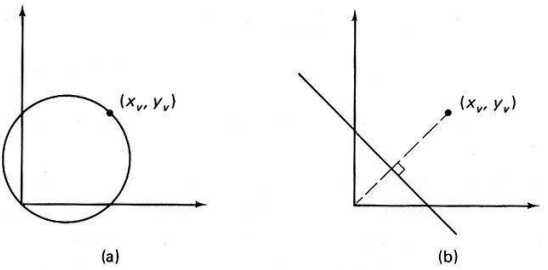

Fig. 6.28 Vanishing point loci.

In Kender's application the texels and their placement tesselation are similar in that the primitives are parallel to arcs in the placement tesselation graph. In a more general application the tesselation could be computed by connecting the centers of primitives.

EXERCISES

6.1 Devise a computer algorithm that, given a set of texels from each of a set of different "windows" of the textured image, checks to see of the resolution is appropriate. In other words, try to formalize the discussion of resolution in Section 6.2.

6.2 Are any of the grammars in Section 6.3 suitable for a parallel implementation (i.e., parallel application of rules)? Discuss, illustrating your arguments with examples or counterexamples from each of the three main grammatical types (shape, tree, and array grammars).

6.3 Are shape, array, and tree grammars context free or context-sensitive as defined? Can such grammars be translated into "traditional" (string) grammars? If not, how are they different; and if so, why are they useful?

6.4 Show how the generalized Hough transform (Section 4.3) could be applied to texel detection.

6.5 In an outdoors scene, there is the problem of different scales. For example, consider the grass. Grass that is close to an observer will appear "sharp" and composed of primitive elements, yet grass distant from an observer will be much more "fuzzy" and homogeneous. Describe how one might handle this problem.

6.6 The texture energy transform (Section 6.4.1) is equivalent to a set of Fourier-domain operations. How do the texture energy features compare with the ring and sector features?

6.7 The texture gradient is presumably a gradient in some aspect of texture. What aspect is it, and how might it be quantified so that texture descriptions can be made gradient independent?

6.8 Write a texture region grower and apply it to natural scenes.

REFERENCES

BAJCSY, R. and L. LIEBERMAN. "Texture gradient as a depth cue." *CGIP 5*, 1, March 1976, 52–67.

BRODATZ, P. *Textures: A Photographic Album for Artists and Designers.* Toronto: Dover Publishing Co., 1966.